

A new lumped structure photochemical mechanism for large-scale applications

Rahul A. Zaveri

Atmospheric Sciences Technical Group, Pacific Northwest National Laboratory, Richland, Washington

Leonard K. Peters

Department of Chemical Engineering, Virginia Polytechnic Institute and State University, Blacksburg

Abstract. The lumped-structure approach for condensing organic chemical mechanisms is attractive, since it yields fewer species and reactions and reduces computational costs. This paper leads through the development of a new lumped-structure mechanism, largely based on the widely used Carbon Bond Mechanism (CBM-IV) developed by *Gery et al.* [1989]. The new mechanism called CBM-Z extends the original framework to function properly at larger spatial and longer timescales. The major modifications in the mechanism include revised inorganic chemistry; explicit treatment of the lesser reactive paraffins, methane and ethane; revised parameterizations of the reactive paraffin, olefin, and aromatic reactions; inclusion of alkyl and acyl peroxy radical interactions and their reactions with NO_3 ; inclusion of organic nitrates and hydroperoxides; and refined isoprene chemistry based on the condensed one-product mechanism of *Carter* [1996]. CBM-Z was successfully evaluated along with the CBM-IV, a partially revised CBM-IV, and a revised Regional Acid Deposition Model (RADM2) mechanism [*Stockwell et al.*, 1990; *Kirchner and Stockwell*, 1996] using the low NO_x and volatile organic compound concentration smog chamber experiments of *Simonaitis et al.* [1997]. Box model versions of the four mechanisms were also evaluated under a variety of hypothetical urban and rural scenarios for a period of 30 days. Results from CBM-Z and revised RADM2 were found to be within $\pm 20\%$ of each other, while CBM-IV and revised CBM-IV results deviated significantly by up to 50–95%. Sensitivity tests were performed to elucidate the effects of some of the new features added in CBM-Z. Relative computational memory and time requirements of these mechanisms are also discussed.

1. Introduction

1.1. Background

Many of the global sulfur cycle models developed in the past employed highly parameterized chemical mechanisms with prescribed NO_x and oxidant fields [*Erickson et al.*, 1991; *Langner and Rodhe*, 1991; *Pham et al.*, 1995; *Chin et al.*, 1996; *Feichter et al.*, 1996]. Although such mechanisms may allow very short simulation turnaround times, and may be particularly attractive for deriving first estimates of the global sulfur budgets, they cannot be used in more prognostic tropospheric chemistry models which predict oxidants, NO_x and other product species based on time varying anthropogenic and biogenic emissions of various trace gases.

The large number of trace gases emitted into the atmosphere may be broadly classified into inorganic and organic compounds. Reactive inorganic gases primarily include NO , NO_2 , SO_2 , and CO , while organic gases of tropospheric interest include thousands of species of both anthropogenic and biogenic origin. While the atmospheric chemistry of the inorganic species is well defined and quite tractable, it is currently unfeasible to treat the organic species individually in a regional or global chemistry model for three major reasons: (1) limited computational resources, (2) lack of detailed speciated emissions inventories, and (3) lack of kinetic and mechanistic information for all the species and their reaction products. Thus there exists a need for a condensed mechanism that is capable of describing the tropospheric hydrocarbon chemistry with reasonable accuracy, sensitivity, and speed at regional to global scales.

During the past two to three decades, many condensed gas phase photooxidation mechanisms have been developed for urban and regional air quality models

Copyright 1999 by the American Geophysical Union.

Paper number 1999JD900876.
0148-0227/99/1999JD900876\$09.00

[Dodge, 1977; Whitten *et al.*, 1980; Atkinson *et al.*, 1982; McRae *et al.*, 1982; Lurmann *et al.*, 1987; Stockwell, 1986; Gery *et al.*, 1989; Carter, 1990; Stockwell *et al.*, 1990]. Some of these mechanisms have continually undergone modifications and improvements resulting from many years of smog chamber experiments and kinetic studies. The modern gas phase chemical mechanisms have thus reached a fairly advanced state of development and understanding. These mechanisms are derived using the same body of kinetic data from which the explicit mechanisms are developed; however, they differ in the simplification techniques, popularly known as the "lumping techniques."

1.2. Lumping Techniques: Advantages and Limitations

In general, three different lumping techniques have been used in the past to simplify the complex organic chemistry of the polluted troposphere: (1) surrogate species [Dodge, 1977], (2) lumped molecule [Atkinson *et al.*, 1982; McRae *et al.*, 1982; Lurmann *et al.*, 1987; Stockwell *et al.*, 1990], and (3) lumped structure [Whitten *et al.*, 1980; Gery *et al.*, 1989]. Of these three techniques, the latter two have been the most popular because of their higher efficiency and accuracy as compared to the surrogate species technique.

In the lumped molecule technique, large numbers of organic compounds are grouped together into a concise set of volatile organic compound (VOC) categories based on similarity in oxidation reactivity and emission magnitudes [Middleton *et al.*, 1990]. Within each category of VOC (e.g., alkanes, alkenes, aromatics, etc.) there are several lumped molecule species that span the required reactivity range. The emitted organic compounds are lumped into these surrogate species of similar reactivity and molecular weight (MW), thereby capturing the initial reactivity of a hydrocarbon mixture quite well. However, this technique may not always conserve carbon mass, for example, a parent surrogate species may oxidize to a product species of the same MW but is actually represented by a lower MW surrogate species. The lumped molecule mechanism developed by Stockwell *et al.* [1990] for the second generation Regional Acid Deposition Model (RADM2) is one of the most widely used mechanism for regional-scale air quality simulations.

On the other hand, the lumped structure approach involves lumping organics according to the types of bonds present in their molecular structures. Thus the chemistry is categorized according to the reactions of similar carbon bonds (paraffinic carbons (C-C), olefinic carbons (C=C), aldehydic carbons (C-CHO), etc.). The major advantage of the structural-lumping approach is that relatively fewer categories are needed to represent the bond groups as compared to the molecular-lumping technique. While this approach conserves carbon mass, it compromises on the initial reactivity of the hydrocarbon mixture, for example, paraffin carbon atoms of

different hydrocarbons may have different reactivities and yield different products but are treated by a single lumped-structure species. The Carbon Bond Mechanism IV (CBM-IV) developed by Gery *et al.* [1989] is the most popular condensed lumped-structure mechanism.

Due to the various assumptions associated with each lumping technique, it is clear that none of the condensed mechanisms can, within parametric uncertainties, exactly simulate the actual photochemistry of the troposphere. At the very best, they may only yield a representative picture of the complex chemistry under any given "real" scenario. Nevertheless, our confidence in such mechanisms may be enhanced if they displayed similar sensitivities and predictability for certain key species such as O₃, OH, NO_x, etc. under a variety of typical atmospheric conditions. Although all condensed mechanisms have been evaluated against a large number of smog chamber experiments carried out at high concentrations (ppm level), their unequivocal evaluation under dilute atmospheric concentrations (ppb to parts per trillion (ppt) levels) has not yet been possible [Simonaitis *et al.*, 1997].

1.3. Scope

Due to its compactness, CBM-IV is an attractive candidate for inclusion in regional- and global-scale models. However, CBM-IV, designed primarily for brief urban-scale studies, does not include or retain some of the long-lived species and their intermediates which may become important under long-range transport (LRT) conditions at larger spatial scales and longer timescales. Additionally, it does not include peroxy radical interactions which may become important under low NO_x conditions. Also, the isoprene mechanism in CBM-IV is quite crude and needs a complete revision. Our objective was to update and extend the CBM-IV mechanism framework to regional- and global-scale applications while maintaining its compactness and efficiency as much as possible. This paper describes the necessary updates and modifications. The resulting mechanism is called CBM-Z and is listed in Tables 1, 2, and 3.

To show that the improvements in the performance of CBM-Z are not merely due to revisions in the rate constants, but also significantly due to the mechanistic modifications, we have contrasted its performance against the published CBM-IV, the partially revised CBM-IV (denoted by CBM-IV(R)), and the revised RADM2 (denoted by RADM2(R)). While both CBM-IV(R) and RADM2(R) have revised inorganic chemistry, the RADM2(R) also has revised hydrocarbon chemistry based on the recommendations of Kirchner and Stockwell [1996]. These mechanisms are first evaluated against representative low VOC and NO_x concentration smog chamber data and then tested under a variety of hypothetical urban and rural tropospheric conditions to elucidate their long-term behavior with

Table 1. Chemical Species in the CBM-Z Mechanism

Species	Symbol
Nitric oxide	NO
Nitrogen dioxide	NO ₂
Nitrate radical	NO ₃
Nitrogen pentoxide	N ₂ O ₅
Nitrous acid	HNO ₂
Nitric acid	HNO ₃
Pernitric acid	HNO ₄
Ozone	O ₃
Excited-state oxygen atom	O(¹ D)
Ground-state oxygen atom	O(³ P)
Hydroxyl radical	OH
Hydroperoxy radical	HO ₂
Hydrogen peroxide	H ₂ O ₂
Carbon monoxide	CO
Sulfur dioxide	SO ₂
Sulfuric acid	H ₂ SO ₄
Methane	CH ₄
Ethane	C ₂ H ₆
Paraffin carbon (> C <)	PAR
Methanol	CH ₃ OH
Formaldehyde	HCHO
Acetaldehyde	ALD2
Acetone	AONE
Methylglyoxal	MGLY
Ethene	ETH
Terminal olefin carbons (C=C)	OLET
Internal olefin carbons (C=C)	OLEI
Toluene	TOL
Xylene	XYL
Cresol and higher MW phenols	CRES
Toluene-hydroxyl radical adduct	TO ₂
Methylphenoxy radical	CRO
High MW aromatic oxidation fragment	OPEN
Isoprene	ISOP
Lumped intermediate	ISOPRD
Lumped organic nitrate	ONIT
Peroxyacyl nitrate	PAN
Formic acid	HCOOH
Higher organic acid	RCOOH
Methyl hydrogen peroxide	CH ₃ OOH
Ethyl hydrogen peroxide	ETHOOH
Higher organic peroxide	ROOH
Methylperoxy radical	CH ₃ O ₂
Ethylperoxy radical	ETHP
Peroxyacyl radical	C ₂ O ₃
Lumped peroxy radical	RO ₂
Acetylmethyl peroxy radical	ANO2
Nitratoalkyl peroxy radicals	NAP
Lumped peroxy radicals	ISOPP
Isoprene-NO ₃ adduct	ISOPN
Lumped peroxy radicals	ISOPO ₂
NO to NO ₂ operator	XO ₂

respect to several key species such as O₃, H₂O₂, NO_x, PAN, etc.

Predictions by CBM-Z and RADM2 are shown to be in better agreement with the smog chamber data than those by CBM-IV and CBM-IV(R). Furthermore, results from CBM-Z and RADM2 are also found to be in much better agreement with each other over longer

timescales (a month), while CBM-IV and CBM-IV(R) predictions show significant deviations after a few days. The causes for improved performance by CBM-Z are explored via a set of sensitivity tests for some of the newly added features in CBM-Z. Relative CPU time and system memory requirements for these mechanisms are also presented.

2. Modifications to CBM-IV

2.1. Inorganic Chemistry

Inorganic gas phase chemistry of the troposphere consists of reactions of ubiquitous inorganic trace gases such as NO_x, SO₂, CO, O₃, H₂O₂, etc. As mentioned earlier, the inorganic tropospheric chemistry representation is rather well defined and is more or less identical in most of the mechanisms available in the recent literature [Lurmann *et al.*, 1987; Gery *et al.*, 1989; Stockwell *et al.*, 1990]; however, some differences exist in the rate constant expressions. To be consistent with the most recent recommendations [DeMore *et al.*, 1997], we have completely revised and updated the inorganic reactions and their rate constants for the CBM-Z mechanism.

2.2. Paraffin Chemistry

Less reactive paraffins such as methane and ethane tend to be omnipresent due to their relatively long chemical lifetimes. Oxidation products of these compounds include highly reactive methylperoxy (CH₃O₂) and ethylperoxy (ETHP) radicals, respectively, which may contribute significantly towards background oxidant cycling [Kirchner and Stockwell, 1996]. Thus their chemistry must be treated explicitly, especially at larger scales. This was achieved by adding the relevant reactions of these species [DeMore *et al.*, 1997] and modifying several of the existing CBM-IV reactions in which the methylperoxy radical was eliminated.

Paraffin carbon atoms in higher alkanes and other nonmethane hydrocarbons (NMHC) are represented by the lumped surrogate species "PAR." Depending on the type of the carbon atom, that is, primary, secondary and tertiary, PAR forms a corresponding alkyl peroxy radical (RO₂) upon reaction with the OH radical. The RO₂ radical is expected to react with NO, NO₂, NO₃, HO₂, and other alkyl peroxy radicals. The CBM-IV mechanism does not retain the RO₂ radical. Only the reaction with NO is implicitly included with the use of an operator species converting NO to NO₂ (XO₂), while the other reactions are simply ignored. The competing reactions of RO₂ are thought to be significant, especially under low NO_x concentrations [Kirchner and Stockwell, 1996]. Consequently, the RO₂ radical chemistry is now treated explicitly as shown below.

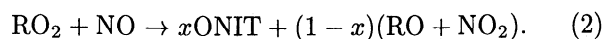
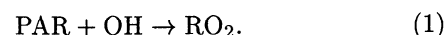


Table 2. Carbon Bond Mechanism (CBM-Z) listing

Reaction Number	Reaction	Rate Constant, k^\dagger	Note
<i>Inorganic Chemistry</i>			
(1)	$\text{NO}_2 + h\nu \xrightarrow{\text{O}_2} \text{NO} + \text{O}({}^3P)$	J_{NO_2}	18
(2)	$\text{NO}_3 + h\nu \rightarrow 0.89\text{NO}_2 + 0.89\text{O}({}^3P) + 0.11\text{NO}$	J_{NO_3}	18
(3)	$\text{HNO}_2 + h\nu \rightarrow \text{OH} + \text{NO}$	J_{HNO_2}	18
(4)	$\text{HNO}_3 + h\nu \rightarrow \text{OH} + \text{NO}_2$	J_{HNO_3}	18
(5)	$\text{HNO}_4 + h\nu \rightarrow \text{HO}_2 + \text{NO}_2$	J_{HNO_4}	18
(6)	$\text{O}_3 + h\nu \rightarrow \text{O}({}^3P)$	$J_{\text{O}_3\text{a}}$	18
(7)	$\text{O}_3 + h\nu \rightarrow \text{O}({}^1D)$	$J_{\text{O}_3\text{b}}$	18
(8)	$\text{H}_2\text{O}_2 + h\nu \rightarrow 2\text{OH}$	$J_{\text{H}_2\text{O}_2}$	18
(9)	$\text{O}({}^1D) + \text{O}_2 \rightarrow \text{O}({}^3P) + \text{O}_2$	$3.2 \times 10^{-11} \exp(70/T)$	1
(10)	$\text{O}({}^1D) + \text{N}_2 \rightarrow \text{O}({}^3P) + \text{N}_2$	$1.8 \times 10^{-11} \exp(110/T)$	1
(11)	$\text{O}({}^1D) + \text{H}_2\text{O} \rightarrow 2\text{OH}$	2.2×10^{-10}	1
(12)	$\text{O}({}^3P) + \text{O}_2 \xrightarrow{\text{M}} \text{O}_3$	$F(6.0(-34), 2.3, 0.0, 0.0)$	1,2
(13)	$\text{O}({}^3P) + \text{O}_3 \rightarrow \text{O}_2 + \text{O}_2$	$8.0 \times 10^{-12} \exp(-2060/T)$	1
(14)	$\text{O}({}^3P) + \text{NO}_2 \rightarrow \text{NO}$	$6.5 \times 10^{-12} \exp(-120/T)$	1
(15)	$\text{O}({}^3P) + \text{NO}_2 \xrightarrow{\text{M}} \text{NO}_3$	$F(9.0(-32), 2.0, 2.2(-11), 0.0)$	1,2
(16)	$\text{O}({}^3P) + \text{NO} \xrightarrow{\text{M}} \text{NO}_2$	$F(9.0(-32), 1.5, 3.0(-11), 0.0)$	1,2
(17)	$\text{O}_3 + \text{NO} \rightarrow \text{NO}_2$	$2.0 \times 10^{-12} \exp(-1400/T)$	1
(18)	$\text{O}_3 + \text{NO}_2 \rightarrow \text{NO}_3$	$1.2 \times 10^{-13} \exp(-2450/T)$	1
(19)	$\text{O}_3 + \text{OH} \rightarrow \text{HO}_2$	$1.6 \times 10^{-12} \exp(-940/T)$	1
(20)	$\text{O}_3 + \text{HO}_2 \rightarrow \text{OH}$	$1.1 \times 10^{-14} \exp(-500/T)$	1
(21)	$\text{OH} + \text{H}_2 \rightarrow \text{HO}_2 + \text{H}_2\text{O}$	$5.5 \times 10^{-12} \exp(-2000/T)$	1
(22)	$\text{OH} + \text{NO} \xrightarrow{\text{M}} \text{HNO}_2$	$F(7.0(-31), 2.6, 3.6(-11), 0.1)$	1,2
(23)	$\text{OH} + \text{NO}_2 \xrightarrow{\text{M}} \text{HNO}_3$	$F(2.5(-30), 4.4, 1.6(-11), 1.7)$	1,2
(24)	$\text{OH} + \text{NO}_3 \rightarrow \text{HO}_2 + \text{NO}_2$	2.2×10^{-11}	1
(25)	$\text{OH} + \text{HNO}_2 \rightarrow \text{NO}_2$	$1.8 \times 10^{-11} \exp(-390/T)$	1
(26)	$\text{OH} + \text{HNO}_3 \xrightarrow{\text{M}} \text{NO}_3$	$k_a + [M]k_b / (1 + [M]k_b/k_c)$ $k_a = 7.2 \times 10^{-15} \exp(785/T)$, $k_b = 1.9 \times 10^{-33} \exp(725/T)$, $k_c = 4.1 \times 10^{-16} \exp(1440/T)$	1,3
(27)	$\text{OH} + \text{HNO}_4 \rightarrow \text{NO}_2$	$1.3 \times 10^{-12} \exp(380/T)$	1
(28)	$\text{OH} + \text{HO}_2 \rightarrow \text{H}_2\text{O} + \text{O}_2$	$4.8 \times 10^{-11} \exp(250/T)$	1
(29)	$\text{OH} + \text{H}_2\text{O}_2 \rightarrow \text{HO}_2$	$2.9 \times 10^{-12} \exp(-160)$	1
(30)	$\text{HO}_2 + \text{HO}_2 \xrightarrow{\text{M}} \text{H}_2\text{O}_2$	$(k_d + [M]k_e)$ $k_d = 2.3 \times 10^{-13} \exp(600/T)$, $k_e = 1.7 \times 10^{-33} \exp(1000/T)$	3,4
(31)	$\text{HO}_2 + \text{HO}_2 + \text{H}_2\text{O} \xrightarrow{\text{M}} \text{H}_2\text{O}_2$	$k_{30} \times 1.4 \times 10^{-21} \exp(2200/T)$	4
(32)	$\text{HO}_2 + \text{NO} \rightarrow \text{OH} + \text{NO}_2$	$3.5 \times 10^{-12} \exp(250/T)$	1
(33)	$\text{HO}_2 + \text{NO}_2 \xrightarrow{\text{M}} \text{HNO}_4$	$F(1.8(-31), 3.2, 4.7(-12), 1.4)$	1,2
(34)	$\text{HO}_2 + \text{NO}_2 \rightarrow \text{HNO}_2$	5.0×10^{-16}	1
(35)	$\text{HNO}_4 \xrightarrow{\text{M}} \text{HO}_2 + \text{NO}_2$	$k_{33} \times 4.76 \times 10^{26} \exp(-10900/T)$	1
(36)	$\text{NO}_3 + \text{NO} \rightarrow 2\text{NO}_2$	$1.5 \times 10^{-11} \exp(170/T)$	1
(37)	$\text{NO}_3 + \text{NO}_2 \rightarrow \text{NO} + \text{NO}_2$	$4.5 \times 10^{-14} \exp(-1260/T)$	1
(38)	$\text{NO}_3 + \text{NO}_2 \xrightarrow{\text{M}} \text{N}_2\text{O}_5$	$F(2.2(-30), 3.9, 1.5(-12), 0.7)$	1,2
(39)	$\text{NO}_3 + \text{NO}_3 \rightarrow 2\text{NO}_2 + \text{O}_2$	$8.5 \times 10^{-13} \exp(-2450/T)$	1
(40)	$\text{NO}_3 + \text{HO}_2 \rightarrow .3\text{HNO}_3 + .7\text{NO}_2 + .7\text{OH}$	3.5×10^{-12}	1
(41)	$\text{N}_2\text{O}_5 + \text{H}_2\text{O} \rightarrow 2\text{HNO}_3$	2.0×10^{-21}	1
(42)	$\text{N}_2\text{O}_5 \xrightarrow{\text{M}} \text{NO}_3 + \text{NO}_2$	$k_{38} \times 3.7 \times 10^{26} \exp(-11000/T)$	1
(43)	$\text{NO} + \text{NO} + \text{O}_2 \xrightarrow{\text{O}_2} 2\text{NO}_2$	$3.3 \times 10^{-39} \exp(530/T)$	5
(44)	$\text{CO} + \text{OH} \xrightarrow{\text{O}_2} \text{HO}_2$	$1.5 \times 10^{-13} (1 + .6P_{\text{atm}})$	1
(45)	$\text{SO}_2 + \text{OH} \rightarrow \text{H}_2\text{SO}_4 + \text{HO}_2$	$F(3.0(-31), 3.3, 1.5(-12), 0.0)$	1,2
<i>Paraffin Chemistry</i>			
(46)	$\text{CH}_4 + \text{OH} \xrightarrow{\text{O}_2} \text{CH}_3\text{O}_2$	$T^{0.667} 2.8 \times 10^{-14} \exp(-1575/T)$	1,10
(47)	$\text{C}_2\text{H}_6 + \text{OH} \rightarrow \text{ETHP}$	$T^2 1.5 \times 10^{-17} \exp(-492/T)$	6,11
(48)	$\text{PAR} + \text{OH} \rightarrow \text{RO}_2$	8.1×10^{-13}	10
(49)	$\text{CH}_3\text{OH} + \text{OH} \rightarrow \text{HCHO} + \text{HO}_2$	$6.7 \times 10^{-12} \exp(-600/T)$	1,11

Table 2. (continued)

Reaction Number	Reaction	Rate Constant, k^\dagger	Note
<i>Carbonyl Chemistry</i>			
(50)	$\text{HCHO} + h\nu \xrightarrow{\text{O}_2} 2\text{HO}_2 + \text{CO}$	J_{HCHOa}	13,18
(51)	$\text{HCHO} + h\nu \rightarrow \text{CO}$	J_{HCHOb}	13,18
(52)	$\text{HCHO} + \text{OH} \xrightarrow{\text{O}_2} \text{HO}_2 + \text{CO}$	1.0×10^{-11}	1,13
(53)	$\text{HCHO} + \text{NO}_3 \xrightarrow{\text{O}_2} \text{HNO}_3 + \text{HO}_2 + \text{CO}$	$3.4 \times 10^{-13} \exp(-1900/T)$	1,13
(54)	$\text{ALD2} + h\nu \xrightarrow{2\text{O}_3} \text{CH}_3\text{O}_2 + \text{HO}_2 + \text{CO}$	J_{ALD2}	10,18
(55)	$\text{ALD2} + \text{OH} \rightarrow \text{C}_2\text{O}_3$	$5.6 \times 10^{-12} \exp(270/T)$	1,13
(56)	$\text{ALD2} + \text{NO}_3 \xrightarrow{\text{O}_2} \text{C}_2\text{O}_3 + \text{HNO}_3$	$1.4 \times 10^{-12} \exp(-1900/T)$	1,13
(57)	$\text{AONE} + h\nu \xrightarrow{2\text{O}_3} \text{C}_2\text{O}_3 + \text{CH}_3\text{O}_2$	J_{AONE}	11,18
(58)	$\text{AONE} + \text{OH} \rightarrow \text{ANO}_2$	$T^2 5.3 \times 10^{-18} \exp(-230/T)$	6,11
(59)	$\text{MGLY} + h\nu \rightarrow \text{C}_2\text{O}_3 + \text{CO} + \text{HO}_2$	$9.64 \times J_{\text{HCHOa}}$	13,17
(60)	$\text{MGLY} + \text{OH} \rightarrow \text{XO}_2 + \text{C}_2\text{O}_3$	1.7×10^{-11}	13
(61)	$\text{MGLY} + \text{NO}_3 \rightarrow \text{HNO}_3 + \text{C}_2\text{O}_3 + \text{CO}$	$1.4 \times 10^{-12} \exp(-1900/T)$	11,12
<i>Olefin chemistry</i>			
(62)	$\text{ETH} + \text{O}_3 \rightarrow \text{HCHO} + 0.22\text{HO}_2 + 0.12\text{OH} + 0.24\text{CO} + 0.24\text{CO}_2 + 0.52\text{HCOOH}$	$1.2 \times 10^{-14} \exp(-2630/T)$	1,14
(63)	$\text{ETH} + \text{OH} \rightarrow \text{XO}_2 + 1.56\text{HCHO} + \text{HO}_2 + 0.22\text{ALD2}$	$F(1.0(-28), 0.8, 8.8(-12), 0.0)$	1,13
(64)	$\text{OLET} + \text{O}_3 \rightarrow 0.57\text{HCHO} + 0.47\text{ALD2} + 0.33\text{OH} + 0.26\text{HO}_2 + 0.08\text{H}_2 + 0.07\text{CH}_3\text{O}_2 + 0.06\text{ETHP} + 0.03\text{RO}_2 + 0.13\text{C}_2\text{O}_3 + 0.04\text{MGLY} + 0.03\text{CH}_3\text{OH} + 0.06\text{CH}_4 + 0.01\text{C}_2\text{H}_6 + 0.31\text{CO} + 0.22\text{CO}_2 + 0.22\text{HCOOH} + 0.09\text{RCOOH} - 1.06\text{PAR}$	$4.2 \times 10^{-15} \exp(-1800/T)$	10,14
(65)	$\text{OLEI} + \text{O}_3 \rightarrow 1.03\text{ALD2} + 0.07\text{AONE} + 0.60\text{OH} + 0.22\text{HO}_2 + 0.10\text{CH}_3\text{O}_2 + 0.05\text{ETHP} + 0.09\text{RO}_2 + 0.11\text{ANO}_2 + 0.19\text{C}_2\text{O}_3 + 0.07\text{MGLY} + 0.04\text{CH}_3\text{OH} + 0.08\text{CH}_4 + 0.01\text{C}_2\text{H}_6 + 0.30\text{CO} + 0.18\text{CO}_2 + 0.16\text{RCOOH} - 2.26\text{PAR}$	$8.9 \times 10^{-16} \exp(-392/T)$	10,14
(66)	$\text{OLET} + \text{OH} \rightarrow \text{XO}_2 + \text{HO}_2 + \text{HCHO} + \text{ALD2} - \text{PAR}$	$5.8 \times 10^{-12} \exp(478/T)$	10
(67)	$\text{OLEI} + \text{OH} \rightarrow \text{XO}_2 + \text{HO}_2 + 0.23\text{AONE} + 1.77\text{ALD2} - 2.23\text{PAR}$	$2.9 \times 10^{-11} \exp(255/T)$	10
(68)	$\text{OLET} + \text{NO}_3 \rightarrow \text{NAP}$	$3.1 \times 10^{-13} \exp(-1010/T)$	10
(69)	$\text{OLEI} + \text{NO}_3 \rightarrow \text{NAP}$	2.5×10^{-12}	10
<i>Aromatic Chemistry</i>			
(70)	$\text{TOL} + \text{OH} \rightarrow 0.08\text{XO}_2 + 0.2\text{HO}_2 + 0.12\text{CRES} + 0.8\text{TO}_2$	$2.1 \times 10^{-12} \exp(322/T)$	10
(71)	$\text{XYL} + \text{OH} \rightarrow 0.5\text{XO}_2 + 0.55\text{HO}_2 + 0.8\text{MGLY} + 1.1\text{PAR} + 0.45\text{TO}_2 + 0.05\text{CRES}$	$1.7 \times 10^{-11} \exp(116/T)$	10
(72)	$\text{TO}_2 + \text{NO} \rightarrow 0.95(\text{NO}_2 + \text{OPEN} + \text{HO}_2) + 0.05\text{ONIT}$	8.1×10^{-12}	13
(73)	$\text{CRES} + \text{OH} \rightarrow 0.4\text{CRO} + 0.6\text{XO}_2 + 0.6\text{HO}_2 + 0.3\text{OPEN}$	4.1×10^{-11}	13
(74)	$\text{CRES} + \text{NO}_3 \rightarrow \text{CRO} + \text{HNO}_3$	2.2×10^{-11}	13
(75)	$\text{CRO} + \text{NO}_2 \rightarrow \text{ONIT}$	1.4×10^{-11}	13
(76)	$\text{OPEN} + \text{OH} \rightarrow \text{XO}_2 + \text{C}_2\text{O}_3 + 2\text{CO} + 2\text{HO}_2 + \text{HCHO}$	3.0×10^{-11}	13
(77)	$\text{OPEN} + h\nu \rightarrow \text{C}_2\text{O}_3 + \text{CO} + \text{HO}_2$	$9.04 \times J_{\text{HCHOa}}$	13,17
(78)	$\text{OPEN} + \text{O}_3 \rightarrow 0.03\text{ALD2} + 0.62\text{C}_2\text{O}_3 + 0.7\text{HCHO} + 0.69\text{CO} + 0.08\text{OH} + 0.03\text{XO}_2 + 0.76\text{HO}_2 + 0.2\text{MGLY}$	$5.4 \times 10^{-17} \exp(-500/T)$	13
<i>Isoprene Chemistry</i>			
(79)	$\text{ISOP} + \text{OH} \rightarrow \text{ISOPP} + 0.08\text{XO}_2$	$2.55 \times 10^{-11} \exp(409/T)$	10,15
(80)	$\text{ISOP} + \text{O}_3 \rightarrow 0.6\text{HCHO} + 0.65\text{ISOPRD} + 0.27\text{OH} + 0.07\text{CO} + 0.39\text{RCOOH} + 0.07\text{HO}_2 + 0.15\text{ALD2} + 0.2\text{XO}_2 + 0.2\text{C}_2\text{O}_3$	$1.2 \times 10^{-14} \exp(-2013/T)$	10,15
(81)	$\text{ISOP} + \text{NO}_3 \rightarrow \text{ISOPN}$	$3.0 \times 10^{-12} \exp(-446/T)$	10,15
(82)	$\text{ISOPRD} + \text{OH} \rightarrow 0.5\text{C}_2\text{O}_3 + 0.5\text{ISOPO}_2 + 0.2\text{XO}_2$	3.3×10^{-11}	15
(83)	$\text{ISOPRD} + \text{O}_3 \rightarrow 0.27\text{OH} + 0.1\text{HO}_2 + 0.11\text{C}_2\text{O}_3 + 0.07\text{XO}_2 + 0.05\text{CH}_3\text{O}_2 + 0.16\text{CO} + 0.15\text{HCHO} + 0.02\text{ALD} + 0.09\text{AONE} + 0.85\text{MGLY} + 0.46\text{RCOOH}$	7.0×10^{-18}	15
(84)	$\text{ISOPRD} + h\nu \rightarrow 0.97\text{C}_2\text{O}_3 + 0.33\text{HO}_2 + 0.33\text{CO} + 0.7\text{CH}_3\text{O}_2 + 0.2\text{HCHO} + 0.07\text{ALD} + 0.03\text{AONE}$	J_{ISOPRD}	15,18
(85)	$\text{ISOPRD} + \text{NO}_3 \rightarrow 0.07\text{C}_2\text{O}_3 + 0.07\text{HNO}_3 + 0.64\text{CO} + 0.28\text{HCHO} + 0.93\text{ONIT} + 0.28\text{ALD2} + 0.93\text{HO}_2 + 0.93\text{XO}_2 + 1.86\text{PAR}$	1.0×10^{-15}	15

Table 2. (continued)

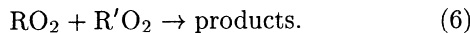
Reaction Number	Reaction	Rate Constant, k^\dagger	Note
<i>Organic Hydroperoxides</i>			
(86)	$\text{CH}_3\text{OOH} + h\nu \xrightarrow{\text{O}_2} \text{HCHO} + \text{HO}_2 + \text{OH}$	$J_{\text{CH}_3\text{OOH}}$	11,18
(87)	$\text{ETHOOH} + h\nu \rightarrow \text{ALD2} + \text{HO}_2 + \text{OH}$	same as reaction (86)	9,11
(88)	$\text{ROOH} + h\nu \rightarrow \text{OH} + 0.4\text{XO}_2 + 0.74\text{AONE} + 0.3\text{ALD2} + 0.1\text{ETHP} + 0.9\text{HO}_2 - 1.98\text{PAR}$	same as reaction (86)	9,11
(89)	$\text{CH}_3\text{OOH} + \text{OH} \rightarrow 0.7\text{CH}_3\text{O}_2 + 0.3\text{HCHO} + 0.3\text{OH}$	$3.8 \times 10^{-12} \exp(200/T)$	1,11
(90)	$\text{ETHOOH} + \text{OH} \rightarrow 0.7\text{ETHP} + 0.3\text{ALD2} + 0.3\text{OH}$	$3.8 \times 10^{-12} \exp(200/T)$	9,11
(91)	$\text{ROOH} + \text{OH} \rightarrow 0.77\text{RO}_2 + 0.19\text{MGLY} + 0.04\text{ALD2} + 0.23\text{OH} - 0.42\text{PAR}$	$3.8 \times 10^{-12} \exp(200/T)$	9,11
<i>Organic Nitrates</i>			
(92)	$\text{ONIT} + \text{OH} \rightarrow \text{NAP}$	$1.6 \times 10^{-11} \exp(-540/T)$	11,12
(93)	$\text{ONIT} + h\nu \rightarrow \text{NO}_2 + 0.41\text{XO}_2 + 0.74\text{AONE} + 0.3\text{ALD2} + 0.1\text{ETHP} + 0.9\text{HO}_2 - 1.98\text{PAR}$	J_{ONIT}	11,18
(94)	$\text{C}_2\text{O}_3 + \text{NO}_2 \rightarrow \text{PAN}$	$F(9.7(-29), 5.6, 9.3(-12), 1.5)$	1,13
(95)	$\text{PAN} \rightarrow \text{C}_2\text{O}_3 + \text{NO}_2$	$k_{94} 1.1 \times 10^{28} \exp(-14000/T)$	1,13
<i>Alkyl and Acyl Peroxy Radical Chemistry</i>			
(96)	$\text{CH}_3\text{O}_2 + \text{NO} \rightarrow \text{HCHO} + \text{HO}_2 + \text{NO}_2$	$3.0 \times 10^{-12} \exp(280/T)$	1,11
(97)	$\text{ETHP} + \text{NO} \rightarrow \text{ALD2} + \text{HO}_2 + \text{NO}_2$	$2.6 \times 10^{-12} \exp(365/T)$	1,11
(98)	$\text{RO}_2 + \text{NO} \rightarrow 0.16\text{ONIT} + 0.84\text{NO}_2 + 0.34\text{XO}_2 + 0.62\text{AONE} + 0.25\text{ALD2} + 0.08\text{ETHP} + 0.76\text{HO}_2 - 1.68\text{PAR}$	4.0×10^{-12}	8,11
(99)	$\text{C}_2\text{O}_3 + \text{NO} \xrightarrow{\text{O}_2} \text{CH}_3\text{O}_2 + \text{NO}_2 + \text{CO}_2$	$5.3 \times 10^{-12} \exp(360/T)$	1,10
(100)	$\text{ANO2} + \text{NO} \rightarrow \text{NO}_2 + \text{C}_2\text{O}_3 + \text{HCHO}$	4.0×10^{-12}	8,11
(101)	$\text{NAP} + \text{NO} \rightarrow 1.5\text{NO}_2 + 0.5\text{HCHO} + 0.5\text{ALD2} + 0.5\text{ONIT} + 0.5\text{HO}_2 - \text{PAR}$	4.0×10^{-12}	8,11
(102)	$\text{ISOPP} + \text{NO} \rightarrow 0.09\text{ONIT} + 0.91\text{NO}_2 + 0.91\text{HO}_2 + 0.63\text{HCHO} + 0.91\text{ISOPRD} + 0.18\text{PAR}$	4.0×10^{-12}	8,15
(103)	$\text{ISOPN} + \text{NO} \rightarrow \text{NO}_2 + 0.8\text{ALD2} + 0.8\text{ONIT} + 0.8\text{HO}_2 + 0.2\text{ISOPRD} + 0.2\text{NO}_2 + 1.6\text{PAR}$	4.0×10^{-12}	8,15
(104)	$\text{ISOPO}_2 + \text{NO} \rightarrow \text{NO}_2 + \text{HO}_2 + 0.59\text{CO} + 0.55\text{ALD2} + 0.25\text{HCHO} + 0.34\text{MGLY} + 0.63\text{AONE}$	4.0×10^{-12}	8,15
(105)	$\text{XO}_2 + \text{NO} \rightarrow \text{NO}_2$	4.0×10^{-12}	8,13
(106)	$\text{CH}_3\text{O}_2 + \text{NO}_3 \rightarrow \text{HCHO} + \text{HO}_2 + \text{NO}_2$	1.1×10^{-12}	7,11
(107)	$\text{ETHP} + \text{NO}_3 \rightarrow \text{ALD2} + \text{HO}_2 + \text{NO}_2$	2.5×10^{-12}	7,11
(108)	$\text{RO}_2 + \text{NO}_3 \rightarrow \text{NO}_2 + 0.4\text{XO}_2 + 0.74\text{AONE} + 0.3\text{ALD2} + 0.1\text{ETHP} + 0.9\text{HO}_2 - 1.98\text{PAR}$	2.5×10^{-12}	7,11
(109)	$\text{C}_2\text{O}_3 + \text{NO}_3 \rightarrow \text{CH}_3\text{O}_2 + \text{NO}_2$	4.0×10^{-12}	8,11
(110)	$\text{ANO2} + \text{NO}_3 \rightarrow \text{NO}_2 + \text{C}_2\text{O}_3 + \text{HCHO}$	1.2×10^{-12}	8,11
(111)	$\text{NAP} + \text{NO}_3 \rightarrow 1.5\text{NO}_2 + 0.5\text{HCHO} + 0.5\text{ALD2} + 0.5\text{ONIT} + 0.5\text{HO}_2 - \text{PAR}$	4.0×10^{-12}	8,11
(112)	$\text{XO}_2 + \text{NO}_3 \rightarrow \text{NO}_2$	2.5×10^{-12}	7,11
(113)	$\text{CH}_3\text{O}_2 + \text{HO}_2 \rightarrow \text{CH}_3\text{OOH}$	$3.8 \times 10^{-13} \exp(800/T)$	1,11
(114)	$\text{ETHP} + \text{HO}_2 \rightarrow \text{ETHOOH}$	$7.5 \times 10^{-13} \exp(700/T)$	1,11
(115)	$\text{RO}_2 + \text{HO}_2 \rightarrow \text{ROOH}$	$1.7 \times 10^{-13} \exp(1300/T)$	8,11
(116)	$\text{C}_2\text{O}_3 + \text{HO}_2 \rightarrow 0.4(\text{RCOOH} + \text{O}_3)$	$4.5 \times 10^{-13} \exp(1000/T)$	1,10
(117)	$\text{ANO2} + \text{HO}_2 \rightarrow \text{ROOH}$	$1.2 \times 10^{-13} \exp(1300/T)$	8,11
(118)	$\text{NAP} + \text{HO}_2 \rightarrow \text{ONIT}$	$1.7 \times 10^{-13} \exp(1300/T)$	8,11
(119)	$\text{ISOPP} + \text{HO}_2 \rightarrow \text{ROOH}$	$1.7 \times 10^{-13} \exp(1300/T)$	8,15
(120)	$\text{ISOPN} + \text{HO}_2 \rightarrow \text{ONIT} + 2\text{PAR}$	$1.7 \times 10^{-13} \exp(1300/T)$	8,15
(121)	$\text{ISOPO}_2 + \text{HO}_2 \rightarrow \text{ROOH}$	$1.7 \times 10^{-13} \exp(1300/T)$	8,15
(122)	$\text{XO}_2 + \text{HO}_2 \rightarrow$	$1.7 \times 10^{-13} \exp(1300/T)$	8,11
<i>Parameterized Reformation Reactions</i>			
(123)	$\text{CH}_3\text{O}_2 \rightarrow 0.66\text{HCHO} + 0.32\text{HO}_2 + 0.34\text{CH}_3\text{OH}$	$k_i^{(1)}, i = \text{CH}_3\text{O}_2$	11,16
(124)	$\text{ETHP} \rightarrow 0.8\text{ALD2} + 0.6\text{HO}_2 + 0.2\text{C}_2\text{H}_6$	$k_i^{(1)}, i = \text{ETHP}$	11,16
(125)	$\text{RO}_2 \rightarrow 0.24\text{XO}_2 + 0.21\text{ALD2} + 0.57\text{AONE} + 0.06\text{ETHP} + 0.54\text{HO}_2 - 1.25\text{PAR}$	$k_i^{(1)}, i = \text{RO}_2$	11,16 11,16
(126)	$\text{C}_2\text{O}_3 \rightarrow \text{CH}_3\text{O}_2 + \text{CO}_2$	$k_i^{(1)}, i = \text{C}_2\text{O}_3$	11,16
(127)	$\text{ANO2} \rightarrow 0.7(\text{C}_2\text{O}_3 + \text{HCHO}) + 0.15(\text{MGLY} + \text{AONE})$	$k_i^{(1)}, i = \text{ANO2}$	11,16
(128)	$\text{NAP} \rightarrow 0.5(\text{NO}_2 + \text{HCHO} + \text{ALD2} + \text{ONIT}) - \text{PAR}$	$k_i^{(1)}, i = \text{NAP}$	11,16

Table 2. (continued)

Reaction Number	Reaction	Rate Constant, k^\dagger	Note
<i>Parameterized Rermutation Reactions (continued)</i>			
(129)	ISOPP \rightarrow ISOPRD	$k_i^{(1)}$, $i = \text{ISOPP}$	11,16
(130)	ISOPN \rightarrow ALD2 + ONIT + 2PAR	$k_i^{(1)}$, $i = \text{ISOPN}$	11,16
(131)	ISOPO ₂ \rightarrow 0.5(ALD2 + AONE)	$k_i^{(1)}$, $i = \text{ISOPO}_2$	11,16
(132)	XO ₂ \rightarrow	$k_i^{(1)}$, $i = \text{XO}_2$	11,16

Notes are 1, Rate constant from *DeMore et al.* [1997]; 2, Troe expression function $F(k_0^{300}, n, k_\infty^{300}, m)$, and numbers of the form 6.0(-34) are to be read as 6.0×10^{-34} ; 3, [M] is the air concentration in (molecule cm^{-3}); 4, Rate constant from *Stockwell* [1995]; 5, Rate constant from *Atkinson et al.* [1992]; 6, Rate constant from *Atkinson* [1994]; 7, Rate constant from *Jenkin et al.* [1997]; 8, Rate constant based on *Kirchner and Stockwell* [1996]; 9, Rate constant assumed same as that for similar reaction of CH_3OOH ; 10, Modified CBM-IV reaction in this work; 11, Reaction added in this work; 12, Rate constant from *Stockwell et al.* [1990]; 13, *Gery et al.* [1989]; 14, This work (R.A. Zaveri, unpublished data, 1998); 15, This work, based on Carter, unpublished mechanism, 1996; 16, Parameterized reaction (see text); 17, Rate constant taken from *Gery et al.* [1988]; 18, See Table 3 for references on photolytic rate data.

[†]The units for rate constants of first-order reactions are s^{-1} ; of second-order reactions, $\text{cm}^3 \text{s}^{-1}$; and for third-order reactions, $\text{cm}^6 \text{s}^{-1}$.



In order to parameterize the organic nitrate (ONIT) yield (x) in (2), we must know the composition and type of the RO_2 radicals resulting from the paraffins. Since the atmospheric higher alkane composition would vary with time and location, a representative mixture is adopted here based on the National Acid Precipitation Assessment Program (NAPAP) anthropogenic alkane emissions inventory [*Placet et al.*, 1991; *Middleton et al.*, 1990] and is shown in Table 4. The composition of the lumped RO_2 radical resulting from this alkane

mix was estimated by the structure-activity relationship method at an average lower tropospheric temperature of 270 K [*Atkinson*, 1987] and was found to consist of 13% 1° RO_2 , 64% 2° RO_2 and 23% 3° RO_2 (also shown in Table 4).

The average ONIT yield was estimated by applying the semiempirical formula of *Carter and Atkinson* [1989] for individual RO_2 radicals. Since the yield is a function of temperature and pressure, a value of $x = 0.16$ is assumed here which is obtained for the approximately average lower tropospheric conditions of $T = 270 \text{ K}$ and $P = 0.8 \text{ atm}$. Loss of ONIT includes photolysis of O- NO_2 bond, and reaction with OH to form nitratoalkyl peroxy radicals (NAP) [*Atkinson*, 1990].

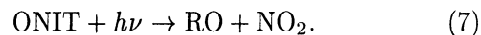


Table 3. References for Photolytic Rate Constant Data

Rate Constant	Absorption Cross Section	Quantum Yield, Φ
J_{NO_2}	<i>DeMore et al.</i> [1997]	<i>DeMore et al.</i> [1997]
J_{NO_3}	<i>Wayne et al.</i> [1991]	<i>Wayne et al.</i> [1991]
J_{HNO_2}	<i>DeMore et al.</i> [1997]	<i>DeMore et al.</i> [1997]
J_{HNO_3}	<i>DeMore et al.</i> [1997]	Assumed to be unity
J_{HNO_4}	<i>DeMore et al.</i> [1997]	Assumed to be unity
$J_{\text{O}_3\text{a}}$	<i>DeMore et al.</i> [1997]	$(1 - \Phi_{\text{O}_3\text{b}})$
$J_{\text{O}_3\text{b}}$	<i>DeMore et al.</i> [1997]	<i>DeMore et al.</i> [1997]
$J_{\text{H}_2\text{O}_2}$	<i>DeMore et al.</i> [1997]	Assumed to be unity
J_{HCHOa}	$\lambda^* < 300 \text{ nm}$, <i>Moortgart et al.</i> [1980] $\lambda > 300 \text{ nm}$, <i>Cantrell et al.</i> [1990]	$\lambda < 300 \text{ nm}$, <i>Atkinson et al.</i> [1997] $\lambda > 300 \text{ nm}$, <i>DeMore et al.</i> [1997]
$J_{\text{HCHO b}}$	Same as for $J_{\text{HCHO a}}$	Same as for $J_{\text{HCHO a}}$
J_{ALD2}	<i>Martinez et al.</i> [1992]	<i>Atkinson et al.</i> [1997]
J_{AONE}	<i>Martinez et al.</i> [1992]	<i>Atkinson et al.</i> [1997]
J_{ISOPRD}	<i>Carter</i> [1996]	<i>Carter</i> [1996]
$J_{\text{CH}_3\text{OOH}}$	<i>DeMore et al.</i> [1997]	<i>DeMore et al.</i> [1997]
J_{ONIT^\dagger}	<i>Atkinson</i> [1994]	<i>Atkinson</i> [1994]

*Variable λ is wavelength of solar radiation.

[†]ONIT assumed to be a mixture of 35% n-propyl nitrate and 65% i-propyl nitrate.

Table 4. Representative Alkane Emission Composition and Estimated RO₂ Yields in the Reaction With OH

Alkane	Fraction ^b	RO ₂ Yields ^a		
		Primary	Secondary	Tertiary
propane	0.0975	0.267	0.733	0.000
<i>n</i> -butane	0.2863	0.120	0.880	0.000
iso-butane	0.0777	0.171	0.000	0.829
<i>n</i> -pentane	0.0473	0.076	0.924	0.000
iso-pentane	0.0897	0.101	0.246	0.653
2,2-dimethylpropane	0.0171	1.000	0.000	0.000
<i>n</i> -hexane	0.0687	0.055	0.945	0.000
2-methylpentane	0.0390	0.076	0.432	0.492
3-methylpentane	0.0231	0.062	0.403	0.535
2,2-dimethylbutane	0.0078	0.354	0.646	0.000
2,3-dimethylbutane	0.0154	0.093	0.000	0.907
<i>n</i> -heptane	0.0690	0.044	0.956	0.000
2-methylhexane	0.0044	0.061	0.544	0.395
3-methylhexane	0.0128	0.056	0.458	0.486
2,4-dimethylpentane	0.0101	0.076	0.185	0.739
<i>n</i> -octane	0.0260	0.036	0.964	0.000
2,2,4-trimethylpentane	0.0426	0.146	0.285	0.568
2,3,3-trimethylpentane	0.0239	0.158	0.230	0.612
4-methylheptane	0.0100	0.048	0.541	0.411
3-methylheptane	0.0084	0.048	0.541	0.411
<i>n</i> -dodecane ^c	0.0226	0.021	0.979	0.000
Total (PAR)	1.0000	0.130	0.640	0.230

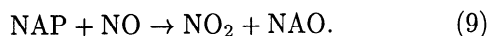
^aEstimated using the technique of *Atkinson* [1987].

^bBased on emissions inventory of *Placet et al.* [1991] and *Middleton et al.* [1990].

^cHigher alkanes are assumed to consist of dodecane.



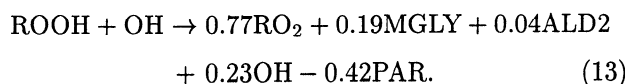
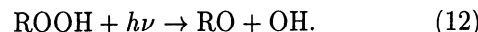
Very little or no experimental data exist for the further loss of NAP. The following reactions are based on the mechanisms proposed by *Atkinson*, [1990].



The subsequent reactions of the nitratealkoxy radicals (NAO) are discussed shortly while the product in (10) is treated as ONIT.

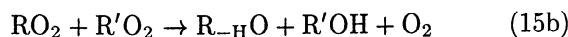
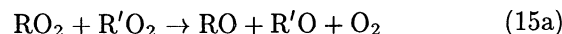
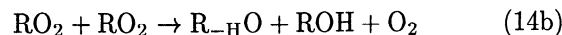
Reaction of RO₂ with NO₂ is rapid, but the peroxy nitrates formed undergo rapid thermal decomposition back to reactants. Thus no overall reaction occurs, and (3) is therefore ignored. Reactions of peroxy radicals with NO₃ can be important especially at nighttime when the NO₃ radicals have appreciable concentrations. These reactions were added based on the study by *Kirchner and Stockwell* [1996].

Organic hydroperoxide (ROOH) formation could not be included in CBM-IV since the RO₂ radical was not retained. It could reach appreciable concentrations in long simulations (weeks to months) and is thought to be important under LRT conditions. Further reactions of ROOH include photolysis and reaction with OH and are based on the recommendations for CH₃OOH [*DeMore et al.*, 1997, and references therein].



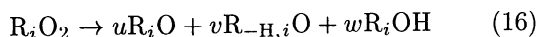
In (13), the formation of higher aldehydes and dicarbonyls are represented by the smallest possible species: acetaldehyde (ALD2) and methylglyoxal (MGLY), respectively. The carbon balance in the reaction is then satisfied by removing an appropriate number of PAR species so that the right-hand side carbon atoms add up to unity. Such approximations are inherent to the carbon bond lumping technique.

An alkylperoxy radical can react with itself and with other alkylperoxy radicals as follows:



For *n* number of alkylperoxy radicals, the total number of self and cross reactions would be $(n^2 + n)/2$, for example, in this mechanism $n = 10$, requiring 55 peroxy-peroxy reactions. To reduce the computational burden

of the mechanism, the $\text{RO}_2 - \text{R}'\text{O}_2$ permutation reactions may be parameterized based on the techniques used by *Madronich and Calvert* [1990] and *Jenkin et al.* [1997] in which each peroxy radical is assumed to react with all other peroxy radicals (i.e., the peroxy radical “pool”) at a single, collective rate. The radical pool is defined as the sum of the concentrations of all peroxy radicals, excluding HO_2 . The collective rate for a given peroxy radical R_iO_2 is represented by a pseudo first-order reaction with a concentration weighted rate constant $k_i^{(1)}$:



$$k_i^{(1)} = \sum_{j=1}^N k_{ij}[\text{R}_j\text{O}_2]. \quad (17)$$

Based on the recommendations of *Jenkin et al.* [1997], the yields in (16) used here are for CH_3O_2 , $u = 0.32$, $v = 0.34$, and $w = 0.34$; for primary and secondary alkylperoxy radicals, $u = 0.6$, $v = 0.2$, and $w = 0.2$; for tertiary alkylperoxy radicals, $u = 0.6$, $v = 0.0$, and $w = 0.4$. The rate constants k_{ij} in (17) are expressed in terms of preexponential factor A_{ij} and activation energy E_{ij}/R as

$$k_{ij} = A_{ij} \exp\left(\frac{-E_{ij}}{RT}\right). \quad (18)$$

The self-reaction rate constants are either available in the literature or can be estimated using the empirical correlation developed by *Kirchner and Stockwell* [1996].

$$k_{ii} = 2 \times 10^{-14} \exp\left(3.8\beta - 5\alpha + \frac{3N}{1 + 0.02N^2}\right), \quad (19)$$

where k_{ii} is the self-reaction rate constant in molecule⁻¹ cm³ s⁻¹; $\beta = 1$ if there are additional oxygen atoms in the alkyl group, while $\beta = 0$ if there are no additional oxygen atoms in the alkyl group; α is the number of alkyl or alkoxy functional groups connected to the C-O-O group; and N is the number of carbon atoms in the alkylperoxy radical, $N \leq 7$. Activation energy for self reactions of alkylperoxy radicals with no additional oxygen atoms are estimated in units of kelvin by

$$E_{ii}/R = 2800\alpha - 700N - 1300, \quad (20)$$

whereas an E_{ii}/R of -1000 K was recommended by *Kirchner and Stockwell* [1996] for alkylperoxy radical self reactions with C-O-O substituent groups that do

Table 5. Estimated Peroxy Radical Permutation Rate Constant Parameters

Radical	CH_3O_2	ETHP	C_2O_3	ANO2	NAP	RO_2	ISOPP	ISOPN	ISOPO2	XO_2
<i>Preexponential Factor ($A_{i,j}$)</i>										
CH_3O_2	2.5(-13) ^a									
ETHP	2.6(-13) ^b	6.8(-14) ^a								
C_2O_3	1.3(-12) ^a	8.9(-13) ^b	2.9(-12) ^a							
ANO2	2.8(-12) ^b	1.5(-12) ^b	9.6(-12) ^b	8.0(-12) ^c						
NAP	1.0(-12) ^b	5.2(-13) ^b	3.4(-12) ^b	5.7(-12) ^b	1.0(-12) ^d					
RO_2	2.3(-14) ^b	1.2(-14) ^b	7.8(-14) ^b	1.3(-13) ^b	4.6(-14) ^b	5.3(-16) ^e				
ISOPP	1.8(-13) ^b	9.2(-14) ^b	6.0(-13) ^b	1.0(-12) ^b	3.5(-13) ^b	8.1(-15) ^b	3.1(-14) ^f			
ISOPN	1.8(-13) ^b	9.2(-14) ^b	6.0(-13) ^b	1.0(-12) ^b	3.5(-13) ^b	8.1(-15) ^b	6.2(-14) ^b	3.1(-14) ^f		
ISOPO2	1.8(-13) ^b	9.2(-14) ^b	6.0(-13) ^b	1.0(-12) ^b	3.5(-13) ^b	8.1(-15) ^b	6.2(-14) ^b	6.2(-14) ^b	3.1(-14) ^f	
XO_2	1.8(-13) ^b	9.2(-14) ^b	6.0(-13) ^b	1.0(-12) ^b	3.5(-13) ^b	8.1(-15) ^b	6.2(-14) ^b	6.2(-14) ^b	6.2(-14) ^b	3.1(-14) ^f
<i>Activation Energy ($-E_{i,j}/R$)</i>										
CH_3O_2	190 ^a									
ETHP	95 ^b	0 ^a								
C_2O_3	640 ^a	250 ^b	500 ^a							
ANO2	95 ^b	0 ^b	250 ^b	0 ^c						
NAP	95 ^b	0 ^b	250 ^b	0 ^b	0 ^d					
RO_2	1085 ^b	990 ^b	1240 ^b	990 ^b	990 ^b	1980 ^e				
ISOPP	595 ^b	500 ^b	750 ^b	500 ^b	500 ^b	1490 ^b	1000 ^f			
ISOPN	595 ^b	500 ^b	750 ^b	500 ^b	500 ^b	1490 ^b	1000 ^b	1000 ^f		
ISOPO2	595 ^b	500 ^b	750 ^b	500 ^b	500 ^b	1490 ^b	1000 ^b	1000 ^b	1000 ^f	
XO_2	595 ^b	500 ^b	750 ^b	500 ^b	500 ^b	1490 ^b	1000 ^b	1000 ^b	1000 ^b	1000 ^f

Values of the form 2.5(-13) are to be read as 2.5×10^{-13} .

^a*DeMore et al.* [1997].

^bCross rate constant parameter calculated by (21) and (22).

^c*Bridier et al.* [1993].

^dAssumed.

^eCalculated by (19) and (20) assuming a representative five-carbon RO_2 composed of 13% primary, 64% secondary, and 23% tertiary radicals.

^fCalculated by (19) assuming a representative five-carbon secondary alkylperoxy radical containing additional oxygen atoms; activation energy ($-E/R$) is assumed equal to 1000 K (see text).

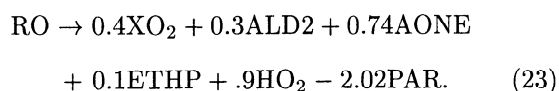
contain oxygen. The cross-reaction rate constant parameters are estimated by

$$A_{ij} = 2\sqrt{A_{ii}A_{jj}} \quad (21)$$

$$E_{ij} = 0.5(E_{ii} + E_{jj}). \quad (22)$$

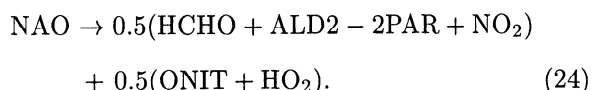
The values of the parameters A_{ij} and E_{ij} used in this work are listed in Table 5. The parameterized first-order reactions are listed in Table 2. A computational strategy for implementing these reactions is discussed in subsection 4.1.

Based on the lumped RO_2 composition, the corresponding lumped alkoxy radical (RO) composition was also determined. Using the rate constants recommended by *Atkinson* [1994], we have assumed that, when possible, the RO radicals undergo rapid isomerization by a 1,5 H-atom shift to give a δ -hydroxy alkyl peroxy radical; if not, then the primary and secondary ROs react with O_2 to give a corresponding carbonyl compound and an HO_2 radical, while the tertiary RO radicals are assumed to undergo thermal decomposition to give a ketone and a smaller alkyl peroxy radical. The resulting lumped RO reaction parameterization is shown below.



Here the formation of δ -hydroxy alkyl peroxy radicals via isomerization of RO are represented by an NO to NO_2 operator species XO_2 . The ketone formed is represented by the smallest possible species: acetone (AONE). As before, the carbon balance is satisfied by subtracting enough PAR so that carbon atoms sum up to unity on the product side.

Loss of nitroalkoxy radicals (NAO) is assumed to occur equally via thermal decomposition giving aldehydes and NO_2 , and reaction with O_2 forming nitroacarbonyls. Instead of adding another species for the nitroacarbonyls, they are represented by ONIT.



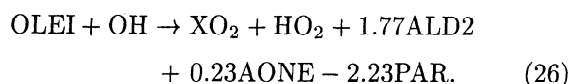
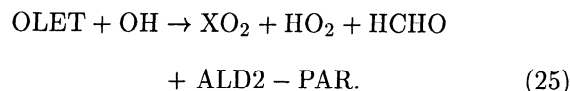
Since the reactions of RO and NAO radicals are always rapid and effectively unimolecular, one can substitute their products in the reactions where they appear as a product. This eliminates all alkoxy radicals in the final mechanism. Subsequent reactions of ALD2, AONE (acetone) and their products are relatively well defined [*DeMore et al.*, 1997; *Atkinson*, 1994] (see Tables 1 and 2 for complete listings).

2.3. Olefin Chemistry

Olefinic carbon bonds are of two types: terminal and internal. Reactions of internal olefins with O_3 proceed about 10 times faster, and with OH about 2 times faster than those for terminal olefins. As a result, internal olefins are much shorter lived than terminal olefins.

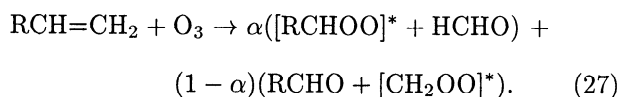
Based on these facts, the CBM-IV developers chose to represent internal olefins directly in terms of their smaller stable carbonyl products (ALD2). However, this approach could potentially introduce significant errors in NO_x as well other oxidant cycles because the reaction products are not always limited to carbonyl compounds. In CBM-Z we represent the terminal and internal olefinic bonds (C=C) by OLET and OLEI, respectively. The remaining paraffin carbons in the compounds are represented by PAR. Ethene is treated explicitly as before. Again, a representative atmospheric olefin composition was constructed based on the NAPAP emissions inventory [*Placet et al.*, 1991; *Middleton et al.*, 1990] and is shown in Table 6. The reactions of OLET and OLEI with OH, O_3 , and NO_3 were parameterized using this mixture.

2.3.1. Reaction with OH radical. The OH radical adds to the double bond forming a β -hydroxy alkyl peroxy radical in the presence of O_2 . Since the olefins emitted from urban sources have much shorter lifetimes between 1 to 5 hours, based on their reactions with OH (1×10^6 molecule cm^{-3}) at 298 K, the β -hydroxy alkyl peroxy radicals resulting from them may experience high NO_x concentrations originating from the same source regions. These peroxy radicals are therefore assumed to react solely with NO to give β -hydroxy alkoxy radicals, which undergo rapid thermal decomposition to form smaller aldehydes. These steps are lumped together as shown below. The intermediate β -hydroxy alkyl peroxy radicals are replaced by XO_2 operator species.

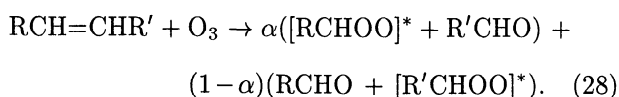


2.3.2. Reaction with ozone. Reactions of olefins with O_3 proceed via the formation of energy-rich Criegee biradicals and carbonyl compounds [*Atkinson*, 1994].

Terminal alkene



Internal alkene



The coefficient α has been measured for a number of unsymmetric alkenes [*Grosjean and Grosjean*, 1997], while $\alpha = 0.5$ for symmetric alkenes by definition. For trisubstituted alkenes ($\text{R}_1\text{CH}=\text{CR}_2\text{R}_3$), the coefficient α is associated with the more substituted biradical $[\text{R}_2\text{C}(\text{OO})\text{R}_3]^*$ and the least substituted primary carbonyl R_1CHO . Table 6 also displays the coefficient α

Table 6. Representative Alkene Emission Composition and Estimated Biradical Yields From Their Ozonolysis Reactions

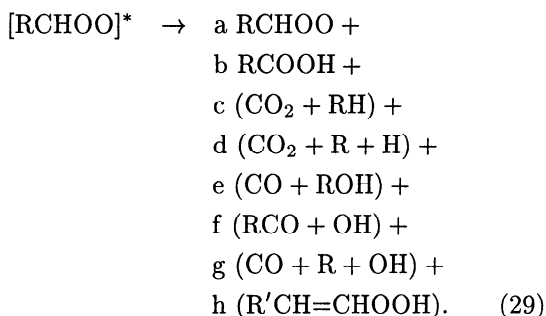
Alkene	Fraction ^a	α^b	Yield [Biradical 1]	Yield [Biradical 2]
Ethene	1.0	0.50	0.50 [CH ₂ OO]*	0.50 [CH ₂ OO]*
<i>Terminal (OLET)</i>				
propenc	0.50	0.56	0.56 [CH ₃ CHOO]*	0.44 [CH ₂ OO]*
1-butene	0.28	0.65	0.65 [C ₂ H ₅ CHOO]*	0.35 [CH ₂ OO]*
1-pentene	0.15	0.50	0.50 [C ₃ H ₇ CHOO]*	0.50 [CH ₂ OO]*
3-methyl-1-butene	0.03	0.50	0.50 [C ₂ H ₅ (CH ₃)CHOO]*	0.50 [CH ₂ OO]*
1-hexene	0.04	0.50	0.50 [C ₄ H ₉ CHOO]*	0.50 [CH ₂ OO]*
<i>Internal (OLEI)</i>				
2-butene	0.24	0.50	0.50 [CH ₃ CHOO]*	0.50 [CH ₃ CHOO]*
2-pentene	0.19	0.50	0.50 [C ₂ H ₅ CHOO]*	0.50 [CH ₃ CHOO]*
2-methyl-2-butene	0.16	0.70	0.70 [CH ₃ C(OO)CH ₃]*	0.30 [CH ₃ CHOO]*
cyclopentene	0.07	0.50	0.50 [OHC C ₃ H ₆ CHOO]*	0.50 [OHC C ₃ H ₆ CHOO]*
2-hexene	0.03	0.50	0.50 [C ₃ H ₇ CHOO]*	0.50 [CH ₃ CHOO]*
3-hexene	0.04	0.50	0.50 [C ₂ H ₅ CHOO]*	0.50 [C ₂ H ₅ CHOO]*
2-methyl-2-pentene	0.07	0.70	0.70 [CH ₃ C(OO)CH ₃]*	0.30 [C ₂ H ₅ CHOO]*
cyclohexene	0.20	0.50	0.50 [OHC C ₄ H ₈ CHOO]*	0.50 [OHC C ₄ H ₈ CHOO]*

^aBased on emission inventory of *Middleton et al.* [1990].

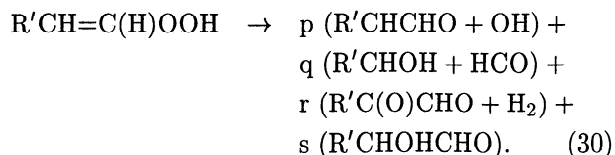
^b*Grosjean and Grosjean* [1997].

and the resulting Criegee biradicals in the ozonolysis of the alkenes in the representative mixture.

The energy-rich Criegee biradicals either collisionally stabilize or thermally decompose giving a variety of radicals and other species. A number of experimental investigations have been carried out in the last two decades to estimate the yields of the decomposition products [*Niki et al.*, 1977, 1981; *Su et al.*, 1980; *Hatakeyama et al.*, 1981, 1984, 1986; *Horie and Moortgart*, 1991; *Atkinson and Aschmann*, 1993; *Atkinson et al.*, 1995; *Horie et al.*, 1994; *Neeb et al.*, 1995, 1996, 1997; *Grosjean and Grosjean*, 1996a,b, 1997; *Grosjean et al.*, 1994, 1996; *Tuazon et al.*, 1997]. Major decomposition channels for a Criegee biradical are thought to include



Further reactions of R'CH=CHOOH are thought to include [*Grosjean et al.*, 1994]



The decomposition channels and product formation yields for the [CH₂OO]* and [CH₃CHOO]* biradicals

were estimated via an extensive computer modeling study of the ethene and *t*-2-butene ozonolysis chemistry. The fates of a few higher Criegee biradicals were also estimated based on the available product formation data (R. A. Zaveri, unpublished data, 1998). The results of that study are summarized here in Table 7. The product formation yields from individual alkenes in the representative mixture were computed using the biradical yields given in Table 6 and the data in Table 7.

Under atmospheric conditions, the stabilized Criegee biradicals (RCHOO) are expected to react predominantly with water vapor to form hydroxyalkyl hydroperoxides (HAHP, HO-R-CHOOH). Data on the further reactions of HAHPs are still highly uncertain. Under laboratory experimental conditions, hydroxymethyl hydroperoxide appears to decompose to formic acid and H₂O presumably involving the reactor surface [*Hatakeyama et al.*, 1981; *Neeb et al.*, 1996, 1997]. No evidence exists on its actual fate in the atmosphere. Until the actual mechanisms are further elucidated, we assume that all HAHPs rapidly decompose to the corresponding organic acids. The final parameterizations for the ozonolysis of OLET and OLEI are listed in Table 2. The dicarbonyls formed in these reactions are represented by methylglyoxal (MGLY).

2.3.3. Reaction with NO₃ radical. Under atmospheric conditions the reaction of alkenes with NO₃ forms β -nitroalkyl peroxy radicals [*Atkinson*, 1994]. This reaction usually becomes important at nighttime when the NO₃ radical concentration may reach appreciable levels while NO levels may drop significantly. Under these conditions, the reactions of β -nitroalkyl peroxy radicals with HO₂ and other peroxy radicals could effectively compete against those with NO. The reaction mechanism is similar to that for the nitroalkyl

Table 7. Estimated Product Yields from Criegee Biradicals Under Atmospheric Conditions

Biradical [RCHOO]*	RCHOO	OH	HO ₂	RH	ROH	RCOOH	RO ₂	RCO ₃	R'CHO ^a	CARB ^b	CO	CO ₂
[CH ₂ OO]*	0.44	0.12	0.22	0.19	0.12	0.08	0.00	0.00	0.00	0.00	0.24	0.24
[CH ₃ CHOO]*	0.20	0.40	0.16	0.20	0.10	0.00	0.25	0.17	0.00	0.07	0.26	0.29
[C ₂ H ₅ CHOO]*	0.12	0.57	0.49	0.07	0.04	0.00	0.26	0.22	0.16	0.13	0.42	0.11
[C ₃ H ₇ CHOO]*	0.08	0.62	0.40	0.08	0.04	0.00	0.31	0.27	0.14	0.08	0.45	0.12
[C ₄ H ₉ CHOO]*	0.05	0.52	0.34	0.17	0.09	0.00	0.30	0.22	0.08	0.09	0.38	0.26
[OCHC ₃ H ₆ CHOO]*	0.05	0.61	0.36	0.12	0.06	0.00	0.31	0.26	0.10	0.10	0.41	0.18
[OCHC ₄ H ₈ CHOO]*	0.03	0.68	0.31	0.16	0.02	0.00	0.30	0.29	0.10	0.10	0.41	0.17
[CH ₃ C(OO)CH ₃]*	0.30	0.70	0.70	0.00	0.00	0.00	0.00	0.00	0.00	0.70	0.00	0.00

R.A. Zaveri (unpublished data, 1998).

^aR'CHO has one carbon atom less than the corresponding [RCHOO]*.

^bCARB represents dicarbonyl compounds such as methylglyoxal.

peroxy radicals (NAP) already discussed. Thus we may model the reactions of OLET and OLEI with NO₃ as expressed as



2.4. Isoprene Chemistry

A number of isoprene photooxidation mechanisms have been proposed since the development of both the CBM-IV and RADM2 mechanisms [Paulson and Seinfeld, 1992; Zimmerman and Poppe, 1996; Carter and Atkinson, 1996]. The detailed mechanism of Carter and Atkinson [1996], implemented for the Statewide Air Pollution Research Center (SAPRC) mechanism [Carter, 1990, 1995], is thought to represent the current state of the art. Based on this mechanism, Carter [1996] developed two condensed versions for inclusion in large-scale simulations: four product mechanism and one product mechanism. Carter also adapted these mechanisms for the RADM2 mechanism [W. P. L. Carter, Isoprene chemistry for the RADM-2 mechanism, letter to the Research Division of the California Air Resources Board, July 11, 1996] (this document is available on the internet at <http://cert.ucr.edu/~carter/bycarter.htm>) (hereinafter referred to as Carter, unpublished mechanism, 1996). Although called a one-product mechanism, the RADM2 version actually consists of four new intermediate species in addition to isoprene itself, and a total of 20 reactions. Introduction of these intermediates and their reactions should make the mechanism more suitable for low-NO_x conditions typical of rural regions where isoprene concentrations may reach appreciable levels.

In this work, we have adapted the one-product mechanism for RADM2 into the CBM framework. Table 8 describes the mapping between RADM2 and CBM species. The adapted isoprene mechanism has the same number of additional intermediate species as in the RADM2 version, however, the self and cross reactions

of the alkylperoxy radicals from isoprene are parameterized as discussed in subsection 2.2. The adapted reactions are listed in Table 2.

2.5. Carbonyl Chemistry

The lumped-structure carbonyl species in the mechanism include acetaldehyde (ALD2), acetone (AONE), and methylglyoxal (MGLY) while HCHO is treated as an explicit species. Loss of these species occur via reactions with OH radical, NO₃ radical, and by photolysis. All reactions of ALD2, AONE, and MGLY eventually lead to an acylperoxy radical represented by C₂O₃. The chemistry of C₂O₃ is based on the reactions of acetylperoxy radical CH₃C(O)O₂.

2.6. Aromatic Chemistry

Not only is the aromatic hydrocarbon chemistry not readily amenable for the lumped-structure condensing approach but is also more complex and poorly understood than most aliphatic hydrocarbon chemistry. The aromatic hydrocarbons of atmospheric importance are represented by two surrogate species TOL and XYL, modeled after toluene and xylene, respectively. The reaction parameterizations derived by Gery *et al.* [1989] are preserved here except for some minor revisions described below.

Based on the results of some recent experimental studies, it appears that cresol yields from the oxidation

Table 8. Equivalent Species Between RADM2 and CBM Mechanisms With Respect to Isoprene Chemistry

RADM2 Species	CBM Equivalent
ACO3	C ₂ O ₃
ALD	ALD2
KET	AONE
ONIT	ONIT + 2PAR
GLY	—
OP2	ROOH
ORA2	RCOOH

of toluene and xylene with OH radical are somewhat overestimated in the CBM-IV mechanism. For example, TOL + OH and XYL + OH reactions contain fixed cresol yields of 36% and 20%, respectively. However, recent experiments of *Atkinson and Aschmann* [1994] show that cresol formation decreases with decreasing initial NO_x concentrations. In the complete absence of initial NO_x, they observed a cresol yield of only 12% from toluene. Since the experimental results are for high NO_x concentrations (ppm levels), it appears that cresol formation from toluene under ambient NO_x levels (ppb), even in a polluted urban environment, would be practically independent of the NO_x channel [*Stockwell et al.*, 1997]. Similarly, a yield of only ~ 5% was estimated from the o-xylene oxidation experiments in the absence of NO_x. Based on these findings, the yields of cresol (CRES) in TOL + OH and XYL + OH were reduced to 12% and 5%, respectively. The corresponding changes in the yields of HO₂ and TO₂ radicals in the above reactions were made accordingly.

We also eliminated the empirical reaction of the TOL-OH adduct TO₂ (with O₂) to produce HO₂ and CRES. This reaction was introduced as a representation for an unknown loss for the TO₂ radical to better fit the high-concentration smog chamber data for toluene. Even with these, the representation of the complex aromatic hydrocarbon chemistry is rather crude and awaits revision as more experimental insights are gained in the future.

3. Mechanism Evaluation With Smog Chamber Data

Although individual reactions in a condensed photochemical mechanism are parameterized using a large

number of experimental studies, it is necessary to evaluate the whole mechanism as a complete system to test its performance and gain confidence in its predictive capability. Ideally, a mechanism should be evaluated under actual atmospheric conditions using field observations. However, this approach is extremely difficult and is greatly complicated by continuously varying meteorological conditions and uncertainties in the emissions of the pollutants. Because of these problems, mechanisms have been traditionally evaluated using both indoor and outdoor smog chambers (also called environmental chambers). Although these are quite useful, they are not free from problems. Some of the most serious limitations include uncertainties in the chamber wall effects and photolysis rates, and the use of relatively high pollutant concentrations than actually found in typical urban or rural air [*Jeffries et al.*, 1987]. Moreover, indoor smog chamber experiments are relatively short (5-10 hours), while outdoor experiments are rarely more than 12 hours long.

There are five major smog chamber data sets available for mechanism evaluation. These are the Dual Outdoor Smog Chamber data set from the University of North Carolina [*Jeffries et al.*, 1982, 1985]; the Indoor Teflon Chamber data set and the Indoor Evacuatable Chamber data set from SAPRC, University of California, Riverside [*Carter et al.*, 1995a, b]; the Dual Outdoor Smog Chamber data set from the Commonwealth Scientific and Industrial Research Organization (CSIRO), Sydney, Australia [*Hess et al.*, 1992a, b, c]; and the Indoor Teflon Chamber data set from the Tennessee Valley Authority (TVA), Muscle Shoals, Alabama [*Simonaitis et al.*, 1997]. The first three data sets consist of high concentration experiments (ppm levels), while the last two are at lower VOC and NO_x concentra-

Table 9. Selected TVA Smog Chamber Experiments

System	Run ^a	[NO], ppb	[NO ₂], ppb	[VOC], ppbC	[VOC]/[NO _x]	Run Time, min	Temperature, K
Formaldehyde	F043094	37.83	3.26	176.45	4.34	120	296.17 - 308.72
Methane	CH4080493	17.78	3.55	124.00 ^b	—	250	297.33 - 309.94
Ethene	E092193	43.14	5.57	243.20	4.99	300	298.17 - 317.61
SynUrban ^c	SU042494	51.12	4.47	498.49	8.97	340	296.28 - 315.72
	SU051694	23.02	1.98	207.73	8.31	420	297.54 - 317.93
	SU042194	23.19	2.18	189.40	7.46	290	297.72 - 322.83
	SU050494	47.53	4.27	375.94	7.26	380	295.67 - 310.33
	SU040894	47.37	4.55	377.66	7.27	360	295.82 - 316.04
	SU041394	46.73	4.80	216.82	4.21	350	296.06 - 317.61
	SU042794	48.32	3.52	203.02	3.92	410	298.32 - 308.54
	SU050994	95.36	8.75	395.94	3.80	300	298.09 - 314.82
	SU051294	70.75	5.74	195.40	2.55	330	300.48 - 314.54

From *Simonaitis et al.* [1997].

^aChamber pressure assumed at 1.05 atm; relative humidity ~ 30%; dilution rate ~ 15% h⁻¹.

^bppm.

^cSynUrban system is a synthetic urban VOC mixture containing 52 hydrocarbon species.

tions (ppb levels). Between the CSIRO and TVA data sets, the latter is more representative of the ambient conditions and also has a well characterized auxiliary wall mechanism, which is essential for evaluating the principal mechanism. Hence we shall use the TVA data set to evaluate the newly developed CBM-Z mechanism.

3.1. Smog Chamber Data and Model Inputs

The TVA data set consists of a series of smog chamber experiments using some key individual VOCs and complex mixtures of VOCs representative of a polluted urban environment [Simonaitis *et al.*, 1997]. Table 9 displays the selected runs that we have used to evaluate CBM-Z. The first three runs are single-component runs of HCHO, CH₄, and ethene, respectively, while the remaining nine runs use a synthetic mixture of 50 volatile organic compounds (SynUrban). The individual components of the SynUrban mixture and their CBM-Z representations are listed in Table 10. The TVA chamber-dependent auxiliary mechanism used in this work is the same as given in Table 3 by Simonaitis *et al.* [1997]. The input data consists of initial concentrations of NO_x, individual VOCs, and time-varying values of temperature, dilution rate, water vapor concentration, and the NO₂ photolysis rate (J_{NO_2}) at 1 min intervals. Photolysis rates of other species were scaled according to the set of values given in Table 4 of Simonaitis *et al.* [1997]. None of the input parameters adjusted to improve the predictions of the principal CBM-Z mechanism.

To elucidate the improvements in CBM-Z's performance due to mechanistic modifications in the organic chemistry, we have contrasted it against the original CBM-IV mechanism [Gery *et al.*, 1989] and also a version of CBM-IV with just the revised inorganic chemistry (same as in CBM-Z) and rate constants, denoted by CBM-IV(R). Also, the XO₂ + HO₂ reaction was added in both CBM-IV and CBM-IV(R) [Simonaitis *et al.*, 1997], and both used the newer peroxyacetyl nitrate (PAN) formation and decomposition rate constants given by DeMore *et al.* [1997]. Furthermore, for an independent check on the performance of CBM-Z, we have also included a revised version of the more detailed RADM2 mechanism in this evaluation exercise. This version of RADM2, denoted by RADM2(R), contained exactly the same inorganic chemistry as in CBM-Z and was also updated based on other relevant recommendations by DeMore *et al.* [1997] and Kirchner and Stockwell [1996]. Furthermore, the isoprene chemistry in the original RADM2 mechanism was also replaced by the one-product mechanism of Carter (unpublished mechanism, 1996).

The system of nonlinear ordinary differential equations describing the dynamic chemistry was solved using LSODES, a GEAR-type solver, on a SUN ULTRA1 workstation. An external model time step of 1 min was used to update the temperature, photolysis rate constants, water vapor concentration, and the dilution rate. The instantaneous values of the species concentra-

Table 10. Species in SynUrban Mixture and Their CBM-Z Representations

Component	CBM-Z Representation
Formaldehyde	HCHO
Acetaldehyde	ALD2
Propene	OLET + PAR
Trans-2-butene	OLEI + 2PAR
Isobutene	OLET + 2PAR
2-methyl-1-butene	OLET + 3PAR
1-pentene	OLET + 3PAR
Cis-2-pentene	OLEI + 3PAR
1,3-butadiene	2OLET
2-methyl-1-pentene	OLET + 4PAR
2-methyl-2-pentene	OLEI + 4PAR
2,3,3-trimethyl-1-butene	OLET + 5PAR
1-octene	OLET + 6PAR
1-monene	OLET + 7PAR
Propane	3PAR
Butane	4PAR
Isobutane	4PAR
Pentane	5PAR
Isopentane	5PAR
2,3-dimethylbutane	6PAR
2-methylpentane	6PAR
3-methylpentane	6PAR
Hexane	6PAR
Methylcyclopentane	6PAR
Cyclohexane	6PAR
2,3-dimethylpentane	7PAR
3-methylhexane	7PAR
Methylcyclohexane	7PAR
Heptane	7PAR
2,2,4-trimethylpentane	8PAR
2,3,4-trimethylpentane	8PAR
2,5-dimethylhexane	8PAR
Octane	8PAR
Nonane	9PAR
Decane	10PAR
4-methylnonane	10PAR
Benzene	TOL
Toluene	TOL
Ethylbenzene	TOL + PAR
m-xylene	XYL
o-xylene	XYL
Propylbenzene	TOL + 2PAR
1,2,4-trimethylbenzene	XYL + PAR
m+p-ethyltoluene	XYL + PAR
sec-butylbenzene	TOL + 3PAR
1,3-diethylbenzene	XYL + 2PAR
1,2,3,5-tetramethylbenzene	XYL + 2PAR
α -methylstyrene	XYL + OLET
Isoprene	ISOP
α -pinene	2ISOP

tions were also printed out every minute. The parameterized first-order reactions of the peroxy radical interactions in CBM-Z were calculated (by equation (17)) using the peroxy radical concentrations at the beginning of each external model time step and assumed to remain constant during the subsequent integration step. This assumption holds good since the peroxy radicals are short lived and hence reach their pseudo-steady

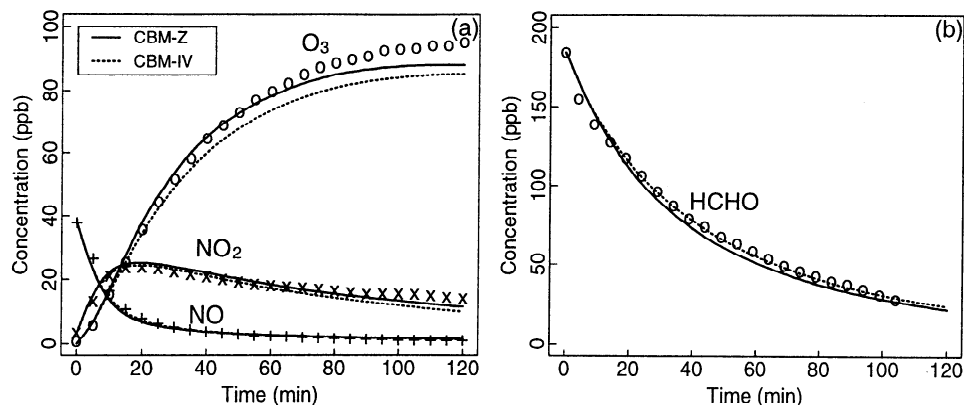


Figure 1. Simulated (lines) and experimental (symbols) profiles for the smog chamber run F043094.

state concentrations very quickly (within 1 to 10 min). Changes in their concentrations are therefore governed by the changes in the concentration of their precursors, which usually have a characteristic time of more than 2-3 hours.

3.2. Results and Discussion

Chemistry of formaldehyde and methane is relatively very simple and well understood. The first two experiments therefore serve to validate the auxiliary wall mechanism and make sure that the principal mechanisms are correctly implemented [Jeffries *et al.*, 1987].

Figure 1 shows the experimental and simulated profiles of O_3 , NO , NO_2 and $HCHO$ for the formaldehyde run F043094. Simulated profiles of only CBM-Z and CBM-IV are plotted because the RADM2(R) and CBM-IV(R) have exactly the same $HCHO$ chemistry and rate constants as in CBM-Z. Although both CBM-Z and CBM-IV show good performance with respect to these species, CBM-Z simulates O_3 slightly better, which can be attributed to the revised inorganic chemistry and rate constants.

The profiles of O_3 , NO , NO_2 , and $HCHO$ from CH_4 oxidation (run CH4080493) are shown in Figure 2. Here

CBM-IV(R) is included in the plot since its methane chemistry treatment is different than in CBM-Z and RADM2(R), the treatment being identical in the latter two. Both CBM-IV and CBM-IV(R) do not retain the intermediate methylperoxy radical formed from $CH_4 + OH$ reaction. CBM-IV slightly underpredicts the rate of O_3 formation while CBM-IV(R) tends to slightly overpredict as compared to the experimental data. CBM-Z appears to predict O_3 quite well until about 200 min, after which all three mechanisms tend to slightly overpredict it. Other species except NO_2 are predicted quite well by all three mechanisms. Consistent overprediction of NO_2 by all three mechanisms may suggest error in measuring total NO_x (i.e., $NO + NO_2$). Nevertheless, good overall agreement with measurements indicate that the wall mechanism is reasonably accurate and the mechanisms were correctly implemented.

Figure 3 shows the experimental and simulated profiles of O_3 , $HCHO$, NO , and NO_2 from ethene photooxidation (run E092193). Here, the simulated profiles from all four mechanisms are plotted since each one behaves differently in the presence of ethene. Both CBM-Z and RADM2(R) are in excellent agreement with respect to the observed ozone and $HCHO$. CBM-IV underpredicts

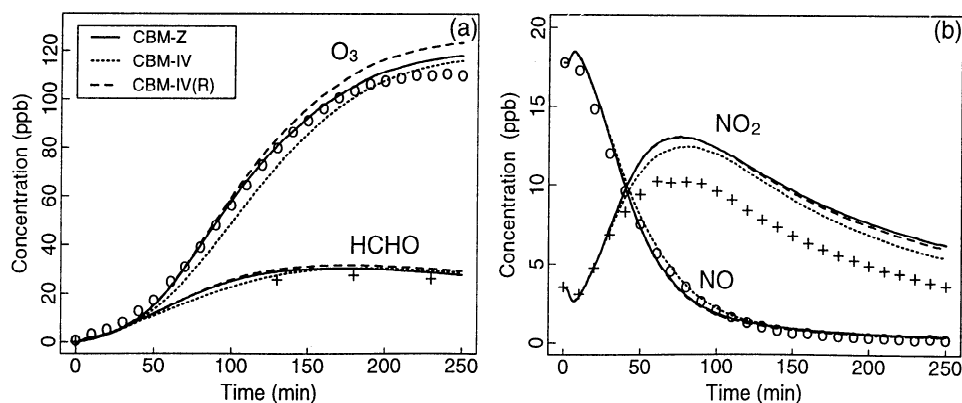


Figure 2. Simulated (lines) and experimental (symbols) profiles for the smog chamber run CH4080493.

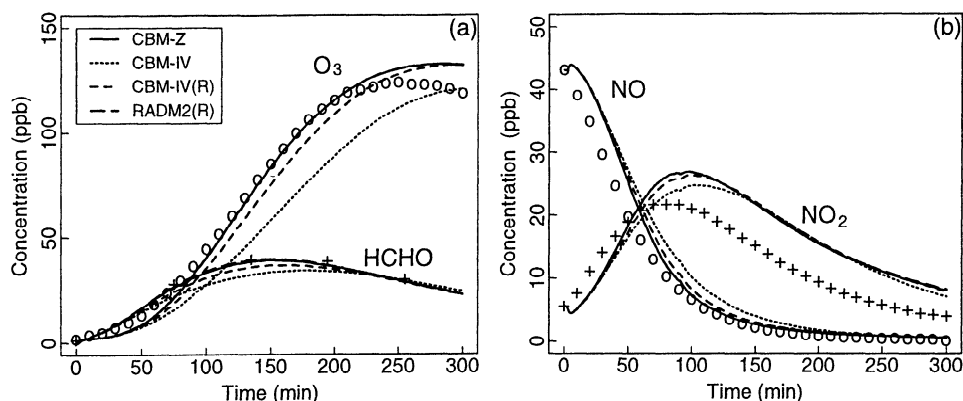


Figure 3. Simulated (lines) and experimental (symbols) profiles for the smog chamber run E092193.

the rate of O₃ formation, while CBM-IV(R) shows significant improvement over CBM-IV. All four mechanisms simulate the NO profile reasonably well. The NO₂ values are overpredicted by all four mechanisms after the NO-NO₂ crossover occurs around $t = 50$ min.

Again, this could be due to some error in the measurements of NO_x than in the predictions.

In summary, the modeled and observed results for the three single-component experiments indicate that both the CBM-Z and RADM2 mechanisms are highly

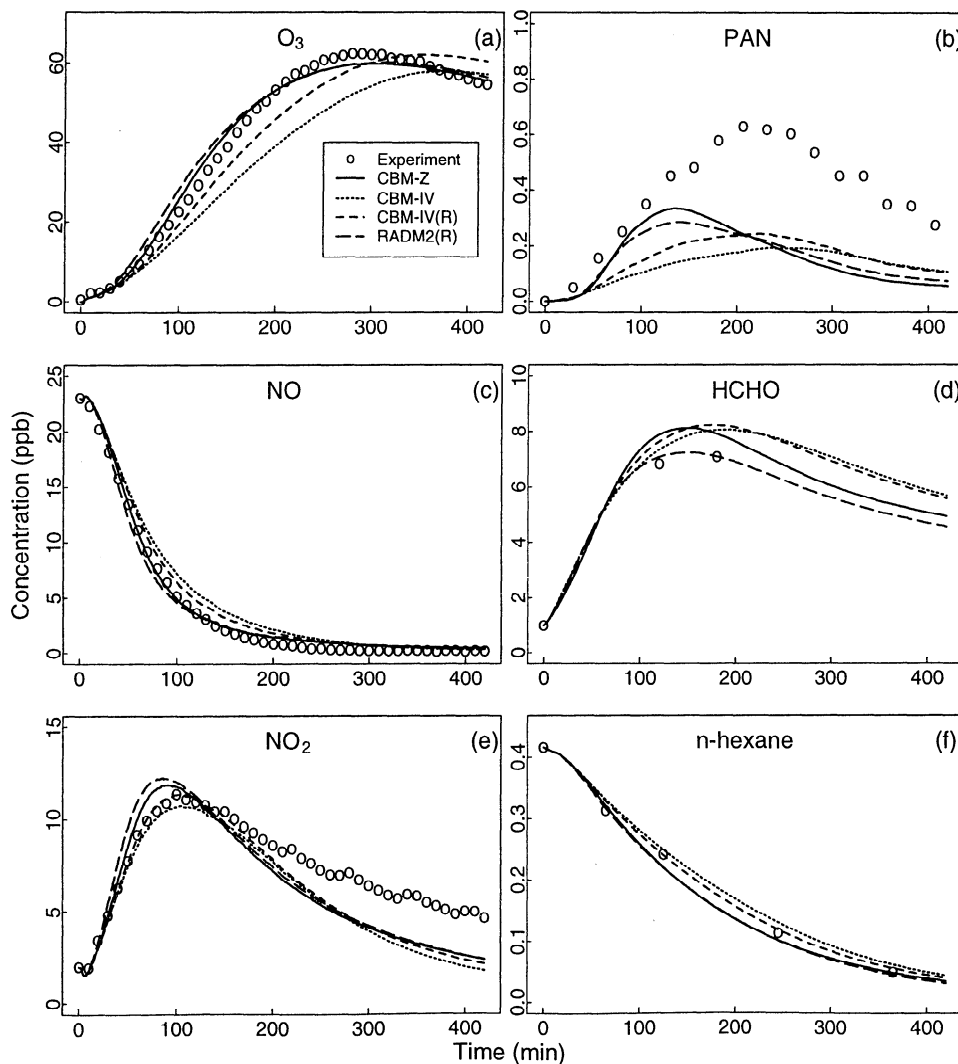


Figure 4. Simulated (lines) and experimental (symbols) profiles for the smog chamber run SU051694.

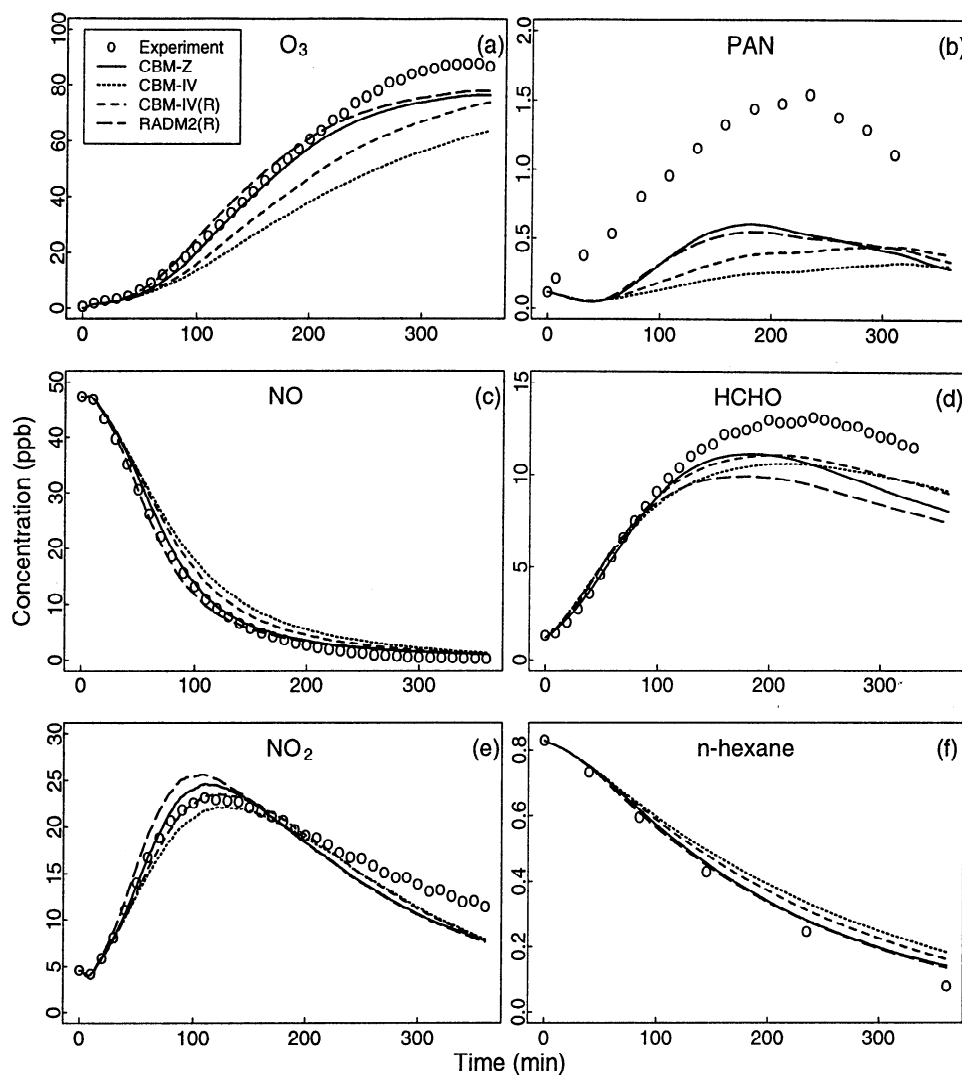


Figure 5. Simulated (lines) and experimental (symbols) profiles for the smog chamber run SU040894.

accurate (within 5% error). And although the original CBM-IV mechanism too performs reasonably well (within experimental errors), its accuracy could be significantly improved just by revising its inorganic chemistry and the rate constants of all the reactions, as reflected in the improved performance of the CBM-IV(R) mechanism.

We shall now present the evaluation of the mechanisms under more representative urban air conditions using the nine SynUrban hydrocarbon mixture experiments. Figures 4 and 5 show the observed and simulated profiles of six key species for the SynUrban runs SU051694 and SU040894, respectively. The predicted O_3 concentrations by CBM-Z and RADM2(R) are in excellent agreement with the measured values for the run SU051694 (Figure 4a). They are also in good agreement for the run SU040894 (Figure 5a) until about 200 min, after which they are somewhat underpredicted by both CBM-Z and RADM2(R). On the other hand, CBM-IV mechanism consistently underpredicts the rate of ozone formation in both the cases, leading to a delay in reach-

ing the maximum value. The CBM-IV(R) mechanism, with revised inorganic chemistry and rate constants, does improve the rate of ozone formation in both the cases but is still somewhat underreactive as compared to CBM-Z and RADM2(R). This fact can also be observed in the NO and NO_2 profiles (Figures 4a and 4b and Figures 5a and 5b). The lower the rate of NO depletion, the slower is the mechanism in producing O_3 .

All four mechanisms severely underpredict PAN concentrations in both the runs by about 50 to 70%. However, unlike CBM-IV and CBM-IV(R), CBM-Z and RADM2(R) do appear to simulate the formation of PAN in the first 100 min quite well for the SU051694 run. All four mechanisms do reasonably well in simulating the HCHO profiles. Last, *n*-hexane, which reacts only with the OH radical, was added in all four mechanisms as a passive reactive species, that is, it reacts with OH but does not have any effect on OH or any other radicals. Thus the observed depletion of *n*-hexane is an indicator of the OH radical concentrations in the chamber. The lower the simulated *n*-hexane con-

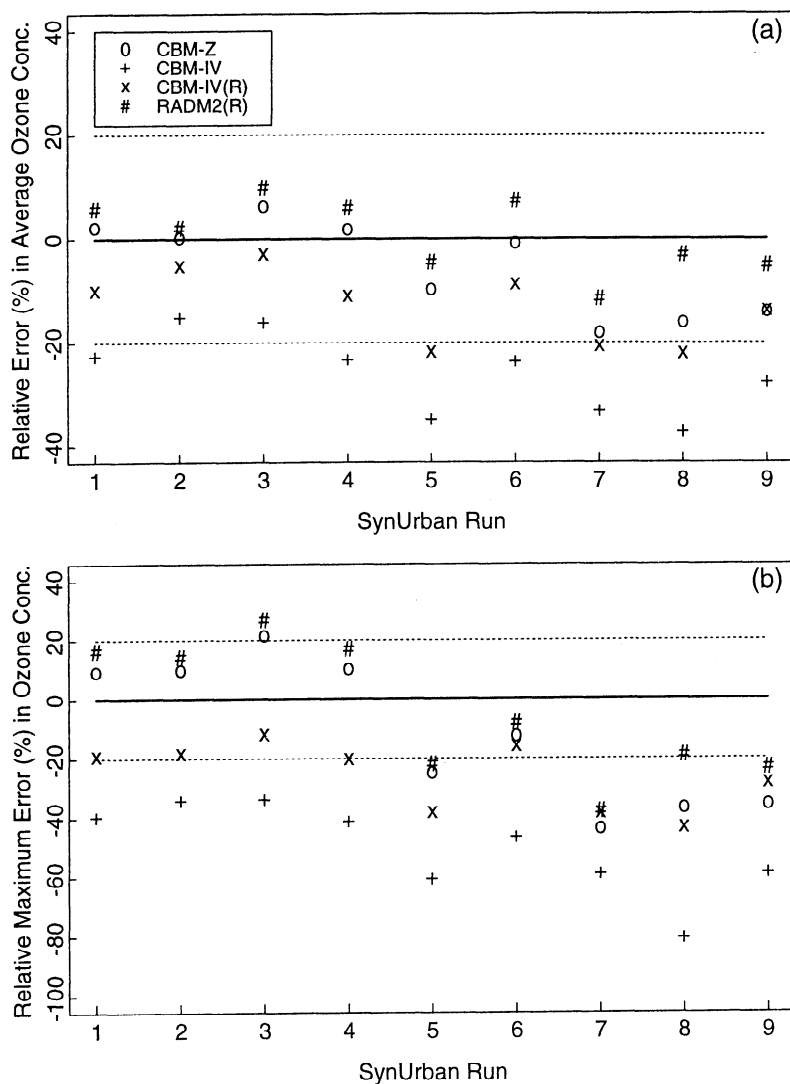


Figure 6. Relative errors between simulated and observed O₃ concentrations in the nine SynUrban runs (a) average and (b) maximum.

centration, the higher is the OH radical concentration predicted by a mechanism. Although all four mechanisms simulate *n*-hexane profiles very well (Figures 4f and 5f), the concentrations predicted by CBM-Z and RADM2(R) are lower than those predicted by CBM-IV, indicating that the CBM-IV mechanism produces lower OH radicals than CBM-Z and RADM2(R). Predictions by CBM-IV(R) lie in between those by CBM-Z and CBM-IV.

Results from all nine SynUrban runs are summarized in Figures 6a and 6b in terms of the percentage relative error in the simulated average O₃ concentrations and percentage relative maximum error in the simulated O₃ concentrations. These are calculated as follows:

$$\%(\text{relative error})_{\text{avg}} = 100 \times \frac{P_{\text{avg}} - O_{\text{avg}}}{O_{\text{avg}}}, \quad (33)$$

$$\%(\text{relative error})_{\text{max}} = 100 \times \frac{\max(P_i - O_i)}{O_{\text{avg}}}, \quad (34)$$

where P_{avg} and O_{avg} are predicted and observed average O₃ concentrations, respectively; and P_i and O_i are the respective instantaneous values sampled at 1 min frequency. The predicted and observed average concentrations were computed using the same number of data points sampled at the same frequency. Also, note that the maximum errors for all mechanisms are computed relative to the average observed O₃ concentration and not the instantaneous observed value where the maximum error occurs. This approach allows us to compare relative maximum errors of different mechanisms on the same basis.

A negative relative error means the mechanism is underpredictive or underreactive. From both the plots, it is clear that CBM-IV is significantly underpredictive with respect to ozone, with the relative average errors ranging between -15% and -37%, and the relative maximum errors ranging between -34% and -81%. This is quite consistent with the conclusions reached by other investigators who have evaluated CBM-IV un-

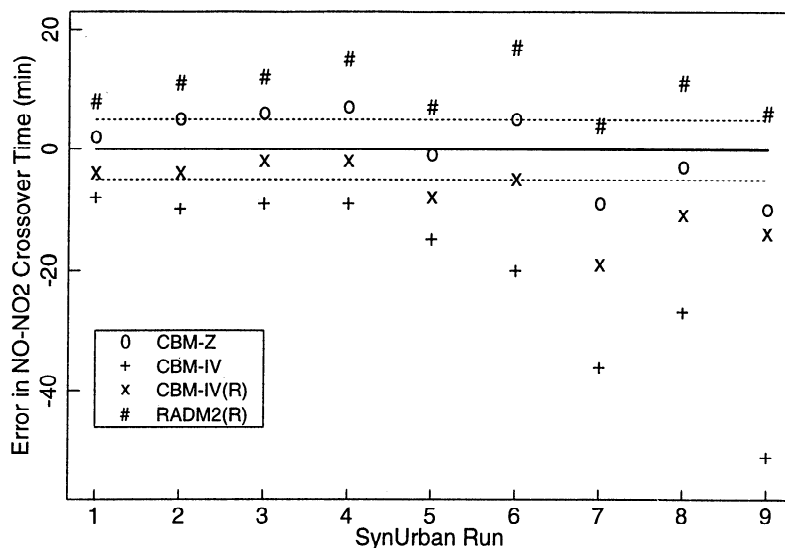


Figure 7. Error in simulated and observed NO-NO₂ crossover times in the nine SynUrban runs.

der relatively low VOC and NO_x conditions [Hess *et al.*, 1992a, b, c]. On the other hand, relative errors (average and maximum) in CBM-IV(R), CBM-Z, and RADM2(R) O₃ predictions are generally within the ±20% error bounds, shown by dotted lines in the plots. However, note that while the relative errors in CBM-Z and RADM2(R) are roughly equally distributed about the zero error line, the errors in CBM-IV(R) are always negative. Although subtle, this is a very important observation which suggests that CBM-IV(R) always tends to be underpredictive and underreactive than CBM-Z and RADM2(R).

Another parameter quite useful in evaluating photochemical mechanisms using smog chamber experiments is the timing of the observed NO-NO₂ crossover point, that is, when the NO and NO₂ concentrations become equal during the course of the experiment. All experiments begin with roughly 90% of the injected NO_x in the form of NO, and rest as NO₂. The NO₂ photolyzes to produce O₃ and NO, while NO is converted back to NO₂ due to its reaction with O₃. However, in the presence of peroxy radicals formed from hydrocarbons, the NO + O₃ reaction must compete with the reaction of NO with peroxy radicals to form NO₂. The net effect is reduction in NO and increase in NO₂ and O₃. The NO-NO₂ crossover time is therefore a good indicator of the rate of formation of peroxy radicals in the early part of the experiment. A delay in the simulated crossover point would mean that the mechanism is underreactive.

Figure 7 shows the plot of errors in the predicted crossover times for the nine SynUrban runs. Here the error is calculated as (observed crossover time) - (predicted crossover time), so that a negative value corresponds to an underreactive system. The crossover time errors in the CBM-Z, CBM-IV, CBM-IV(R) and RADM2 mechanisms range between -10 and +7 min, -8 and -51 min, -2 and -14 min, and +4 and +17 min, respectively. Again, note that both CBM-IV and

CBM-IV(R) are always underreactive, while the errors in CBM-Z are roughly evenly distributed about the zero error line. Interestingly, consistently positive errors in RADM2(R) indicate that it is always overreactive in the early part of the experiment.

In sum, the analyses presented in this section show that CBM-IV is severely underreactive, while CBM-IV(R) is somewhat underreactive with respect to ozone formation. On the other hand, CBM-Z and RADM2(R) are found to be in much better agreement with the experimental data. They do not display any overall tendency to be underreactive or overreactive; however, RADM2 does tend to be somewhat overreactive in the early part of the experiments, at least until the NO-NO₂ crossover occurs. All four mechanisms simulate the HCHO profiles reasonably well. Furthermore, although CBM-Z and RADM2(R) simulate the PAN profiles better than CBM-Z and CBM-IV(R) can, they still underpredict the average concentrations by about 50%.

As mentioned earlier, the smog chamber experiments are of relatively short duration and therefore cannot help fully reveal different mechanisms' behaviors on longer timescales, and under more realistic conditions. One must therefore resort to long-term mechanism intercomparisons to elucidate their subtle, but important, differences.

4. Mechanism Intercomparison

This section presents the comparison of the CBM-Z, CBM-IV, CBM-IV(R), and RADM2(R) mechanisms under a variety of urban and rural scenarios simulated for 30 days.

4.1. Box Model Construction and Inputs

A constant-volume box model was constructed for each mechanism (i.e., with a constant mixing height) to eliminate the effects of entrainment on predictions

Table 11. Anthropogenic Nonmethane Organic Carbon (NMOC) Composition Based on NAPAP Emissions Inventory

NMHC Species <i>i</i>	Species <i>i</i> mole fraction	mole C per mole NMHC	mole <i>i</i> per mole NMOC
Ethane	0.0560	0.1120	0.0121
Propane	0.0504	0.1512	0.0109
C ₄ alkanes	0.1848	0.7392	0.0399
C ₅ alkanes	0.0784	0.3920	0.0169
C ₆ alkanes	0.0784	0.4704	0.0169
C ₇ alkanes	0.0448	0.3136	0.0097
C ₈ alkanes	0.0560	0.4480	0.0121
C ₁₂ alkanes	0.0112	0.1344	0.0024
Ethene	0.1564	0.3128	0.0338
Propene	0.0184	0.0552	0.0040
C ₅ terminal alkenes	0.0184	0.0920	0.0040
C ₅ internal alkenes	0.0368	0.1840	0.0080
Toluene	0.0870	0.6090	0.0188
Xylene	0.0630	0.5040	0.0136
Formaldehyde	0.0400	0.0400	0.0086
C ₃ aldehydes	0.0100	0.0300	0.0021
Acetone	0.0050	0.0150	0.0011
C ₅ ketones	0.0050	0.0250	0.0011
Total	1.0000	4.6278	1.0000

of certain species; dry deposition of gases was also neglected for the same reason. The effects of initial concentrations on the predictions were eliminated by initializing the simulations with zero NO_x and non-methane hydrocarbon (NMHC) concentrations. The only initially nonzero species were O₃, CO, and CH₄ specified at 30, 100, and 1600 ppb, respectively. NO_x and NMHCs were emitted into the box at a prescribed flux which varied diurnally as parameterized below

$$E_i = E_{1,i} \times \cos(\theta_z) + E_{2,i} \quad \forall \cos(\theta_z) \geq 0, \quad (35)$$

$$E_i = E_{2,i} \quad \forall \cos(\theta_z) < 0, \quad (36)$$

where E_i is the emission flux for the i th species, and θ_z is the theoretical solar zenith angle at any given latitude, longitude, and local time. Equations (35) and (36) represent the daytime and nighttime fluxes, respectively. In actual practice, the flux parameters E_1 and E_2 were specified for NO_x and SO₂ only, while the emissions of the NMHCs were calculated using a prescribed [NMOC]/[NO_x] molar ratio (NMOC stands for nonmethane organic carbon). Ninety percent of the total NO_x emitted was in the form of NO, and the remainder as NO₂. A constant water vapor concentration of 3.8×10^{17} molecule cm⁻³, corresponding to 50% relative humidity at 298 K, was also prescribed.

The urban anthropogenic NMOC composition based on NAPAP emissions inventory is shown in Table 11. Using the recommended partitioning rules [Gery *et al.*, 1989] (also see examples in Table 10), the emitted species were apportioned into the surrogate species for each mechanism and are shown in Table 12. Nine hypothetical urban and rural scenarios with varying emission

strengths were used to compare the performance of the mechanisms. The emission flux parameters for these scenarios are listed in Table 13.

Each simulation was performed for 30 model days beginning at 0000 hours, July 1 and at 40°N, 0°E location. A constant mixing height of 1000 m was used for the entire run, while a diurnal variation of temperature (290 K - 304 K) representative of the continental Northern Hemisphere July conditions was prescribed. An external model time step of 1 hour was prescribed at which the temperature, emission fluxes, solar zenith angle, and the parameterized permutation reaction rate constants were updated and kept constant for the subsequent integration step by LSODES. Daily average concentrations of various key species were computed for comparison.

4.2. Results and Discussion

Performance of an atmospheric chemistry mechanism strongly depends on its ability to accurately predict concentrations of the major oxidants such as O₃, H₂O₂, NO₃, NO₂, OH, and HO₂. Predictions of the concentrations of other species such as H₂SO₄, HNO₃, PAN, organic acids, etc., directly or indirectly depend on the reactions of their precursors with the above oxidants. The urban scenario U5 is selected here to illustrate the long-term behavior of the four mechanisms. Figure 8 displays the daily average concentration plots of H₂SO₄, HNO₃, NO₂, PAN, O₃, and H₂O₂. We shall first briefly review the major differences in the predictions and then attempt to explore the underlying reasons by conducting several sensitivity tests on the CBM-Z mechanism.

Production of H₂SO₄ is directly proportional to the OH radical concentrations. As shown in the plots,

Table 12. Nonmethane Organic Carbon Apportionment Into the Organic Surrogates for Each Mechanism

CBM-IV		CBM-Z		RADM2	
Species <i>i</i>	mole <i>i</i> per mole NMOC	Species <i>i</i>	mole <i>i</i> per mole NMOC	Species <i>i</i>	mole <i>i</i> per mole NMOC
PAR	0.6242	C ₂ H ₆	0.0121	C ₂ H ₆	0.0121
		PAR	0.6160	HC3	0.0495
				HC5	0.0327
				HC8	0.0233
ETH	0.0338	ETH	0.0338	OL2	0.0338
OLE	0.0080	OLET	0.0080	OLT	0.0080
		OLEI	0.0080	OLI	0.0080
TOL	0.0188	TOL	0.0188	TOL	0.0188
XYL	0.0136	XYL	0.0136	XYL	0.0136
HCHO	0.0086	HCHO	0.0086	HCHO	0.0086
ALD2	0.0181	ALD2	0.0021	ALD2	0.0021
		AONE	0.0022	KET	0.0013

the daily average H₂SO₄ concentrations and therefore the OH radical concentrations predicted by CBM-Z and RADM2(R) are in excellent agreement, while both CBM-IV and CBM-IV(R) tend to underpredict these species after about 5-6 days. Unlike gas phase H₂SO₄ production, HNO₃ formation is more complex involving various oxides of nitrogen and organic species. Again, the daily average HNO₃ concentrations from CBM-Z and RADM2(R) are in very good agreement, while CBM-IV and CBM-IV(R) results show significant underprediction after a couple of days.

Table 13. Hypothetical Emissions Scenarios

Scenario	NO _x and SO ₂		Isoprene		<i>R</i> _{HC}
	<i>E</i> ₁	<i>E</i> ₂	<i>E</i> ₁	<i>E</i> ₂	
U1	4	1	0	0	10
U2	4	1	0	0	20
U3	4	1	0	0	30
U4	16	4	0	0	10
U5	16	4	0	0	20
U6	16	4	0	0	30
U7	32	8	0	0	10
U8	32	8	0	0	20
U9	32	8	0	0	30
R1	1	0	5	0	10
R2	1	0	20	0	10
R3	1	0	80	0	10
R4	4	1	5	0	10
R5	4	1	20	0	10
R6	4	1	80	0	10
R7	8	2	5	0	10
R8	8	2	20	0	10
R9	8	2	80	0	10

Emissions parameters *E*₁ and *E*₂ are in μmol m⁻² h⁻¹, and *R*_{HC} is the molar ratio of anthropogenic NMOC to NO_x.

The O₃ concentration evolution predicted by CBM-Z and RADM2(R) agree very well, but those predicted by CBM-IV and CBM-IV(R) are significantly lower after about 4 to 5 days. On the other hand, the NO₂ profiles between the two groups start deviating right from the first day. Last, the H₂O₂ concentrations predicted by CBM-IV and CBM-IV(R) are about twice as much as those predicted by CBM-Z and RADM2(R).

For further comparison the daily average concentrations of ONIT, HCHO, CH₃OOH, higher organic hydroperoxides, HCOOH and higher organic acids predicted by CBM-Z and RADM2 for the same scenario are plotted in Figure 9. The two mechanisms produce comparable daily average concentrations of these species (except for the lumped organic nitrates): within 10% deviation after 10 days of simulation, and within 50% deviation after 30 days. At the end of 30 days, the lumped organic nitrate concentrations predicted by CBM-Z are about 4 times higher than those predicted by RADM2. These differences are probably due to the different treatments of the organic nitrate - OH reaction products in RADM2 and CBM-Z. The treatment in CBM-Z is based on the more recent experimental data of organic nitrate reactions (as discussed in subsection 2.2).

Results obtained for all nine urban scenarios are summarized in Figure 10 in terms of relative deviations in the final daily average species concentrations predicted by CBM-Z, CBM-IV, and CBM-IV(R) with respect to the corresponding RADM2 predictions. As seen in the plots, the relative deviations for CBM-Z are well within the ±20% bounds (shown by dotted lines), while those for CBM-IV and CBM-IV(R) deviate significantly from zero. For example, final concentrations of H₂SO₄, HNO₃, NO₂, PAN, and O₃ are generally underpredicted by up to 50 to 90%, while H₂O₂ concentrations are overpredicted by 90 to 150%.

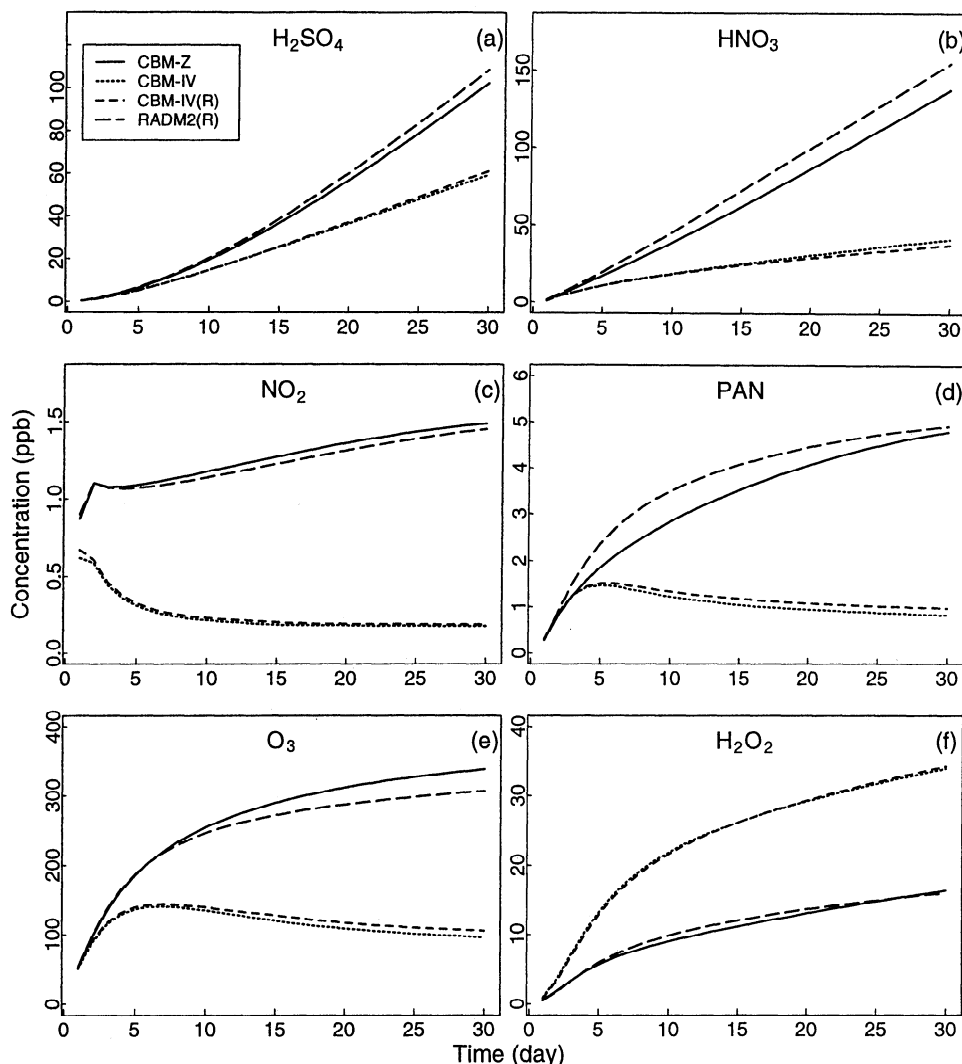


Figure 8. Comparison of CBM-Z, CBM-IV, CBM-IV(R), and RADM2(R) predictions for the urban scenario U5.

These results clearly show that merely revising the inorganic chemistry in CBM-IV does not significantly change its performance under typical atmospheric conditions at longer timescales. To quantitatively elucidate the effects of some of the new features in CBM-Z, we performed a series of five sensitivity tests as described in Table 14. The new CBM-Z features selected for the tests were the reactions of organic peroxides, organic nitrates, alkyl and acyl peroxy radical + NO_3 reactions, interactions of alkyl and acyl peroxy radicals. The Each test involved turning specific reactions off and repeating the simulation for the previously used urban scenario U5. The tests results are contrasted against those from the full CBM-Z mechanism in Figure 11.

Interestingly, H_2SO_4 , and therefore OH radical concentration, appears to be rather insensitive to all the features tested. However, HNO_3 and NO_2 concentrations are most sensitive to the reactions of organic nitrates (test 2) and relatively less sensitive to the reac-

tions of alkyl and acyl peroxy radicals with NO_3 (test 3). Organic nitrates are relatively long lived and therefore act as temporary reservoirs of NO_2 . They can photolyze and react with OH to release the "trapped" NO_2 back into the system. By forming organic nitrates, but ignoring their reactions, a significant fraction of NO_x is permanently lost from the system, thereby lowering the concentrations of NO_2 , HNO_3 and PAN. Lower NO_x concentrations ultimately translate into lower O_3 concentrations seen in Figure 11e for test 2. However, we did not see enough lowering of NO_2 and O_3 as might be expected according to the CBM-IV results we saw in Figures 8b to 8e. This is because the old parameterizations in CBM-IV purged about 67% more NO_x in the form of organic nitrates than in CBM-Z, which made the system extremely underreactive. In the real troposphere, long-range transport of organic nitrates can lead to enhanced O_3 production at a rural downwind location from a primary urban NO_x source. Reactions

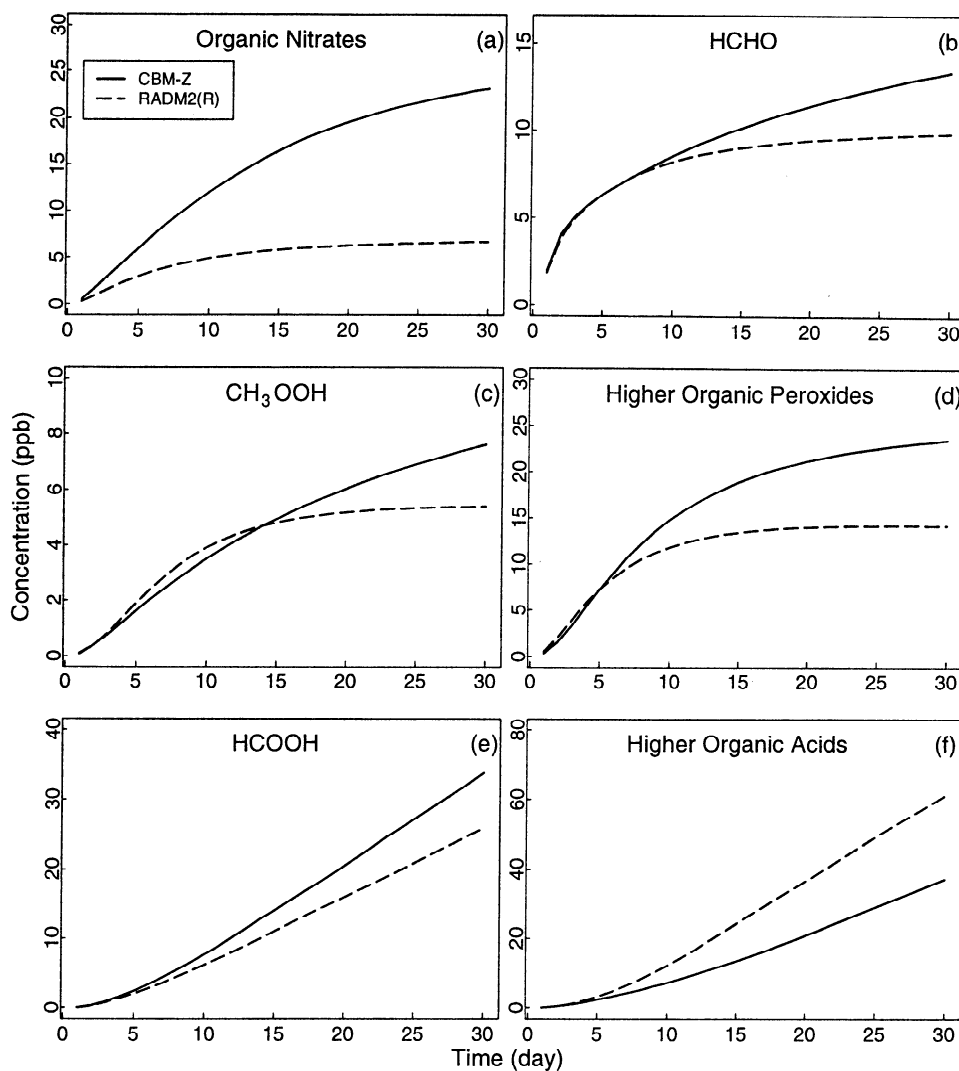


Figure 9. Comparison of CBM-Z and RADM2(R) predictions for the urban scenario U5.

of organic nitrates must be therefore included in large-scale and long-term tropospheric chemistry simulations.

On the other hand, neglecting alkyl and acyl peroxy radical interactions increases their own concentrations and therefore lead to increased PAN and O₃ formation (test 4). Higher alkyl peroxy radical concentrations also mean lower HO₂ radical concentrations by virtue of their reactions 113 through 122 in Table 2. And lower HO₂ levels lead to lower H₂O₂ concentrations, as dictated by reactions (30) and (31) in the same table. Effects of the organic hydroperoxide reactions (test 1) are most pronounced on the levels of H₂O₂. Like organic nitrates, organic hydroperoxides are reservoirs of OH and HO₂ radicals, and other reactive species. Ignoring their reactions tend to decrease the HO₂ radical concentrations and hence decrease the H₂O₂ levels.

Effects of all the above features were simultaneously tested in test 5. Interestingly, some features tend to compensate each other, while others amplify their ef-

fects on the concentrations of the key species. In conclusion, these tests prove that revisions made in the paraffin, olefin, and aromatic reaction parameterizations together with the above tested features must be responsible for the overall improvement in the performance of CBM-Z in comparison to the performance of the original CBM-IV.

Next, the rural scenario R5 is selected here for comparing the predictions of the isoprene chemistry in the four mechanisms. Figure 12 displays the daily average concentrations of H₂SO₄ and HNO₃, O₃, H₂O₂, NO₂, and lumped intermediate ISOPRD. Predictions of these species by CBM-Z and RADM2(R) are in excellent agreement, thus indicating successful mapping of Carter's one-product isoprene mechanism into the CBM-Z framework. As expected, the old isoprene chemistry in both CBM-IV and CBM-IV(R) compares rather poorly, especially with respect to NO₂, O₃, HNO₃, and H₂O₂.

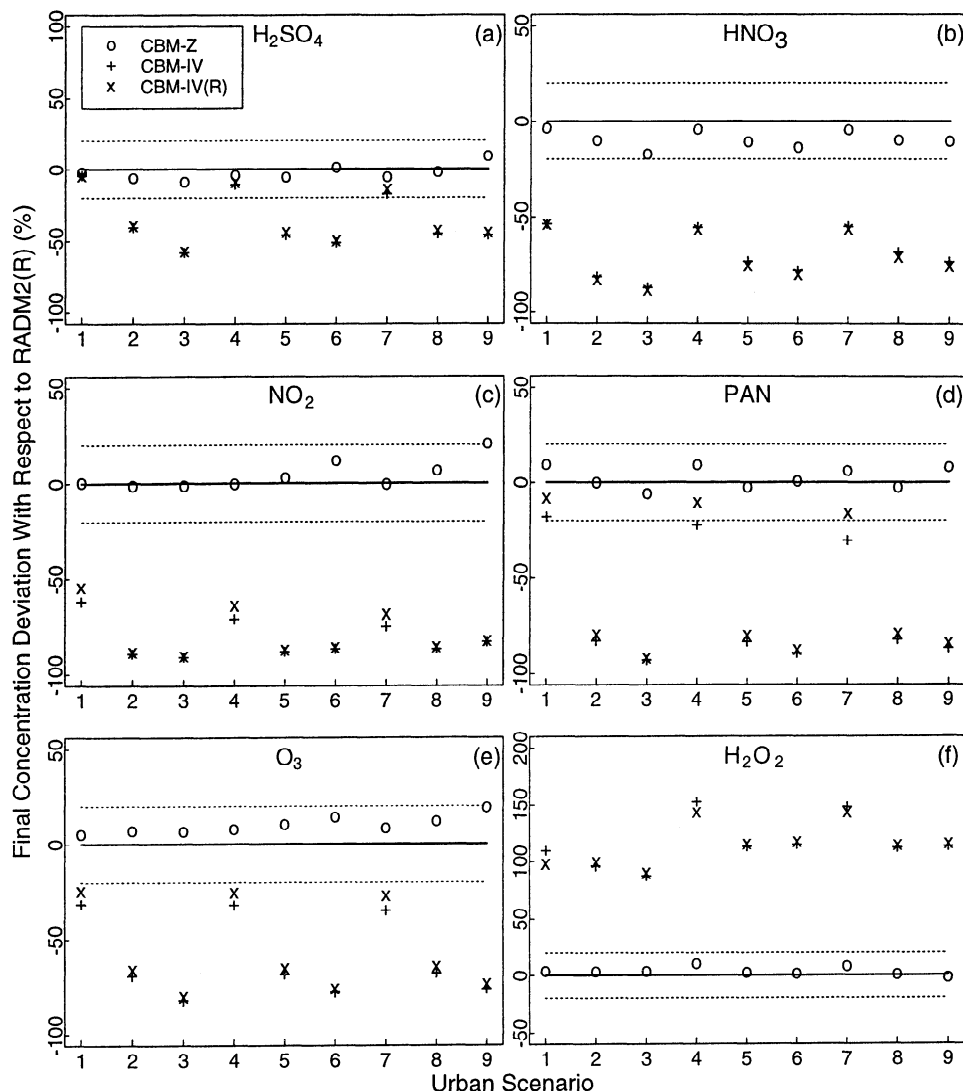


Figure 10. Relative deviations in final concentrations predicted by CBM-Z, CBM-IV, and CBM-IV(R) with respect to RADM2(R) predictions for all nine urban scenarios.

The results from the rest of the rural scenarios are summarized in Figure 13 in terms of the relative deviations of the final daily average species concentrations predicted by CBM-Z, CBM-IV and CBM-IV(R) with respect to the corresponding RADM2(R) predictions. Again, the relative deviations for the CBM-Z predictions are close to zero (within ± 20 -30%) while those for CBM-IV and CBM-IV(R) deviate significantly from

-98% for NO_2 , O_3 , and HNO_3 up to 250% for H_2O_2 . Apart from the problems in the old isoprene mechanism, the underlying reasons for such drastic deviations are same as discussed for the urban scenario U5.

In sum, the CBM-Z and RADM2(R) mechanisms, developed using different lumping techniques, display remarkably similar characteristics and sensitivities in predicting various oxidants and stable species. The CBM-

Table 14. Sensitivity Tests Performed on the CBM-Z Mechanism

Test	New CBM-Z Feature	Reactions Turned Off in Table 2
Test 1	Reactions of organic hydroperoxides	(86) through (88)
Test 2	Reactions of organic nitrates	(92) and (93)
Test 3	Reactions of alkyl and acyl peroxy radicals with NO_3	(106) through (113)
Test 4	Interactions of alkyl and acyl peroxy radicals	(123) through (132)
Test 5	All of the above	All of the above

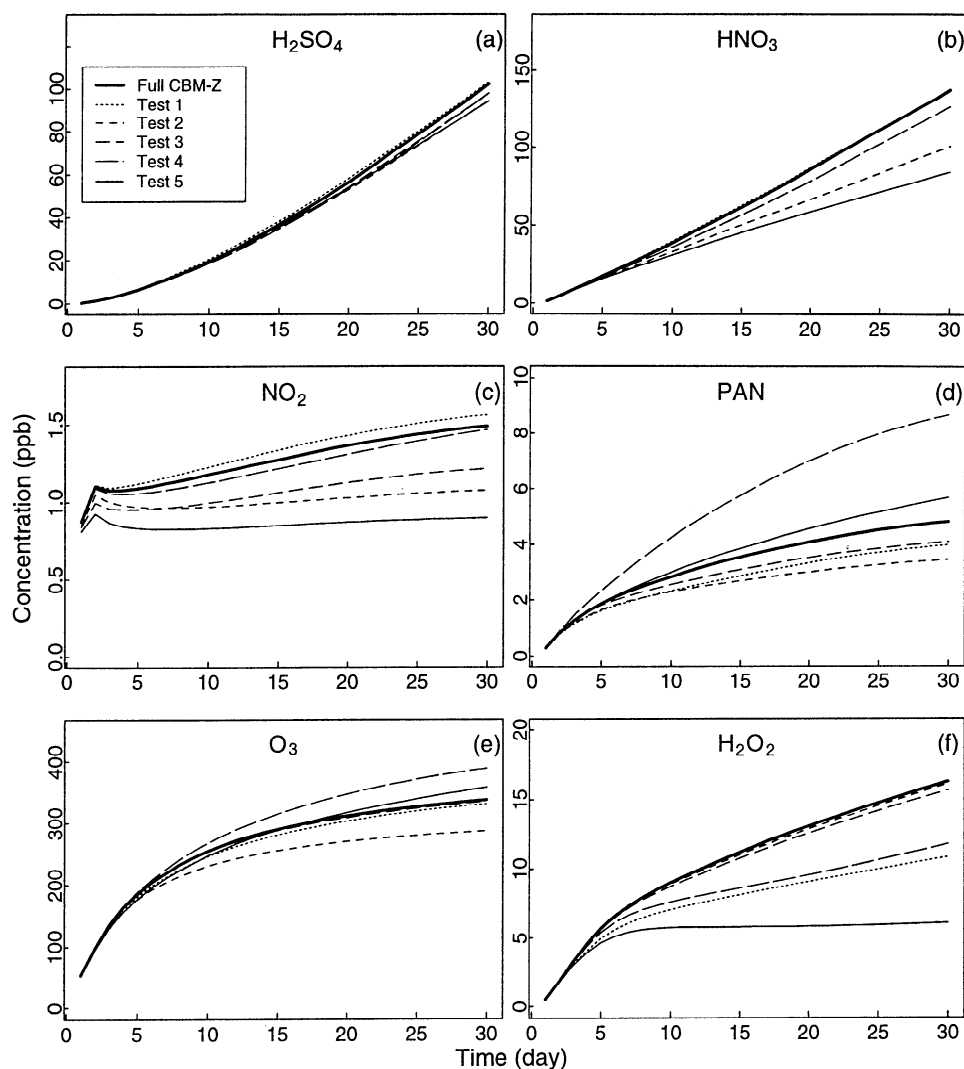


Figure 11. Sensitivity tests on CBM-Z for the urban scenario U5.

IV mechanism, on the other hand, behaves quite differently, especially at timescales longer than 3 - 4 days.

The computational times required to simulate 30 model days were measured for the four mechanisms. As expected, CBM-IV and CBM-IV(R) needed approximately the same time for the same simulation. Along with the average CPU cost relative to that required by RADM2(R), Table 15 summarizes the total number of species and reactions in the RADM2(R), CBM-Z and CBM-IV mechanisms. CBM-Z and CBM-IV require 20% and 46% less system memory, respectively, and are about 25% and 50% faster to execute than RADM2.

5. Summary

The published CBM-IV mechanism, based on the lumped-structure condensing approach, was modified and updated to simulate anthropogenic hydrocarbons and isoprene at regional to global scales. The major modifications involved explicit treatment of lesser reactive paraffins such as methane and ethane; revised pa-

rameterizations of the more reactive paraffins, olefins, and aromatics; explicit treatment of alkylperoxy radical reactions; addition of the NO_3 -alkyl and acyl peroxy radical reactions; detailed treatment of various organic nitrates and organic hydroperoxides; and revised isoprene chemistry based on Carter's one-product mechanism. The resulting mechanism, called CBM-Z, contains 31 organic species and 72 organic reactions in addition to the explicit inorganic chemistry.

The CBM-Z and CBM-IV mechanisms were first evaluated using the TVA smog chamber experiments performed at low VOC and NO_x concentrations (ppb levels). Revised versions of CBM-IV and RADM2, denoted by CBM-IV(R) and RADM2(R), respectively, were also evaluated to better contrast the improvements in the newly developed CBM-Z mechanism. The four mechanisms were then evaluated under a variety of hypothetical urban and rural tropospheric scenarios to elucidate their long-term behavior with respect to several key species.

The O_3 concentrations and NO_x profiles simulated by

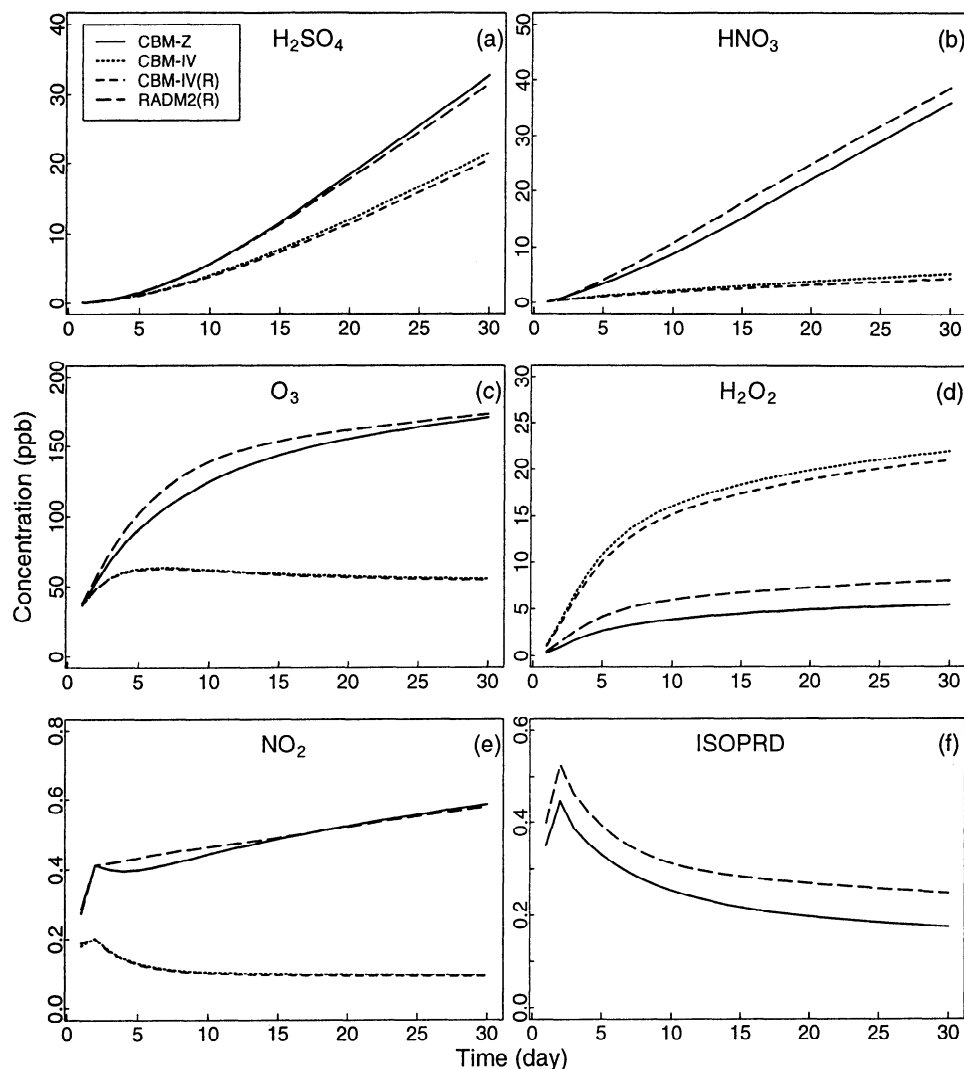


Figure 12. Comparison of CBM-Z, CBM-IV, CBM-IV(R), and RADM2(R) predictions for the rural scenario R5.

CBM-Z and RADM2 were found to be in better agreement, generally within $\pm 20\%$, with the smog chamber data than those produced by CBM-IV and CBM-IV(R). The latter were consistently underreactive for all the nine experiments using a synthetic urban hydrocarbon mixture. All four mechanisms were able to simulate the HCHO profiles reasonably well but significantly underpredicted the PAN concentrations by 50–70%. However, the shape of the PAN profiles and the maximum concentrations predicted by CBM-IV and RADM2 were in better agreement with the observations than those simulated by CBM-IV and CBM-IV(R).

The long-term simulated H_2SO_4 , HNO_3 , O_3 , NO_2 , PAN and H_2O_2 profiles by CBM-Z and RADM2 were also found to be in much better agreement with each other under both urban and rural scenarios (well within $\pm 20\%$), while the CBM-IV and CBM-IV(R) predictions started deviating significantly after about 1–3 days. After 30 days, the daily average concentrations of these species from CBM-Z and RADM2 were still within

$\pm 20\%$, while those (except H_2O_2) from CBM-IV and CBM-IV(R) were significantly lower by 50–95%. The H_2O_2 concentrations predicted by the latter two were about 50% higher.

The causes for improved performance of CBM-Z were explored via a set of sensitivity runs which tested the effects of some of the newly added features in CBM-Z. The reactions of organic nitrates and alkyl peroxy radical interactions had the most pronounced effects on the concentrations of NO_2 and O_3 . Furthermore, it was found that the revised reaction parameterizations in CBM-Z lowered the yields of organic nitrates by about 67% than in CBM-IV. Moreover, ignoring their reactions in CBM-IV caused a significant fraction of NO_x to be removed from the system permanently, which otherwise may have been recycled. Reactions of organic hydroperoxides also had appreciable effects on H_2O_2 concentrations. These “reservoir” species can be transported over long distances and lead to enhanced O_3 and H_2O_2 production away from the primary NO_x sources

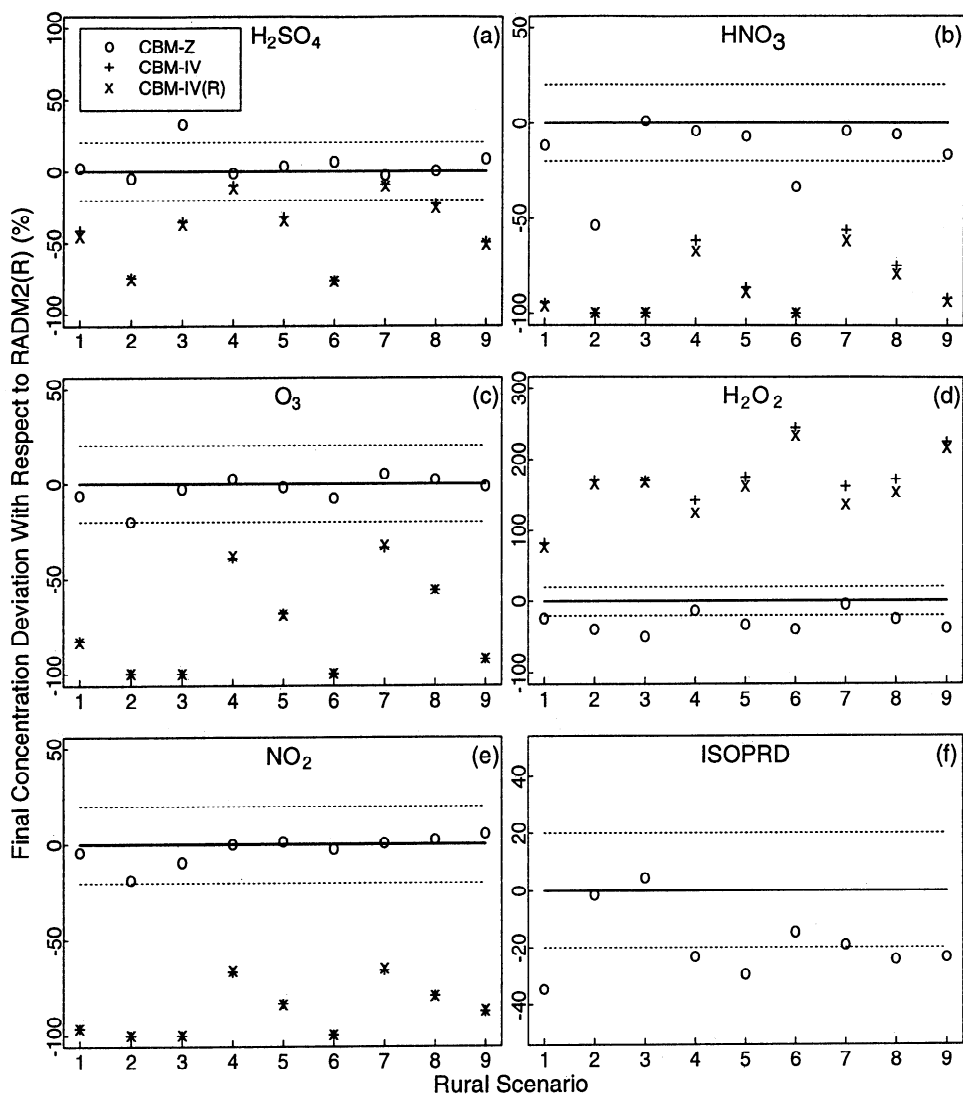


Figure 13. Relative deviations in final concentrations predicted by CBM-Z, CBM-IV, and CBM-IV(R) with respect to RADM2(R) predictions for all nine rural scenarios.

by releasing NO₂, HO₂, and other radicals in the presence of sunlight.

Relative CPU time and system memory requirements for these mechanisms were calculated. The overall CBM-Z mechanism is approximately 20% smaller than RADM2(R) in terms of the total number of species, and about 25% faster than RADM2(R) to execute. Such memory and time savings are always critical for large-scale three-dimensional simulations, especially with finer grid resolutions.

Table 15. Mechanism Statistics

Mechanism	Total Species	Total Reactions	Average CPU Cost Relative to RADM2
RADM2	65	198	1.00
CBM-Z	52	132	0.75
CBM-IV	35	83	0.50

Acknowledgments. R.A.Z. would like to thank W. Richard Barchet, Carl M. Berkowitz, Richard C. Easter, Steve J. Ghan, Pius C. S. Lee, Rick D. Saylor, and Yang Zhang for many valuable discussions throughout the progress of this work. The authors are grateful to Harvey Jeffries and Zachariah Adelman at the University of North Carolina, Chapel Hill, for sharing the electronic copies of the TVA smog chamber data sets. The authors are also grateful to the two anonymous referees for their comments and suggestions. Funding for this work was provided through the U.S. EPA Aerosol Program under contract CR822079-01-0 and by the NASA Aerosol Program under contracts NAGW 3367 and NAS5-98072. R.A.Z. is also grateful to Associated Western Universities NW for awarding a postgraduate fellowship. Pacific Northwest National Laboratory is operated for DOE by Battelle Memorial Institute under contract DE-AC06-76RLO 1830.

References

Atkinson, R., A structure-activity relationship for the estimation of rate constants for the gas-phase reactions of OH radicals with organic compounds, *Int. J. Chem. Kinet.*, 19, 799-828, 1987.

- Atkinson, R., Gas-phase tropospheric chemistry of organic compounds: A review, *Atmos. Environ.*, **24A**, 1-41, 1990.
- Atkinson, R., Gas-phase tropospheric chemistry of organic compounds: A review, *J. Phys. Chem. Ref. Data*, Monogr., **2**, 1-216, 1994.
- Atkinson, R., and S. M. Aschmann, OH radical production from the gas-phase reactions of O₃ with a series of alkenes under atmospheric conditions, *Environ. Sci. Technol.*, **27**, 1357-1363, 1993.
- Atkinson, R., and S. M. Aschmann, Products of the gas-phase reactions of aromatic hydrocarbons: Effect of NO₂ concentration, *Int. J. Chem. Kinet.*, **26**, 929-944, 1994.
- Atkinson, R., D. L. Baulch, R. A. Cox, R. F. Hampson Jr., J. A. Kerr, M. J. Rossi, and J. Troe, Evaluated kinetic, photochemical and heterogeneous data for atmospheric chemistry: Supplement V, IUPAC subcommittee on gas kinetic data evaluation for atmospheric chemistry, *J. Phys. Chem. Ref. Data*, **26**(3), 521-1012, 1997.
- Atkinson, R., D. L. Baulch, R. A. Cox, R. F. Hampson Jr., J. A. Kerr, and J. Troe, Evaluated kinetic, photochemical and heterogeneous data for atmospheric chemistry: Supplement IV, IUPAC subcommittee on gas kinetic data evaluation for atmospheric chemistry, *J. Phys. Chem. Ref. Data*, **21**(6), 1125-1568, 1992.
- Atkinson, R., A. C. Lloyd, and L. Wings, An updated chemical mechanism for hydrocarbon/NO_x/SO₂ photooxidations suitable for inclusion in atmospheric simulation models, *Atmos. Environ.*, **16**, 1341-1355, 1982.
- Atkinson, R., E. C. Tuazon, and S. M. Aschmann, Products of the gas-phase reactions of O₃ with alkenes, *Environ. Sci. Technol.*, **29**, 1860-1866, 1995.
- Bridier, I., B. Veyret, R. Lesclaux, and M. E. Jenkin, Flash photolysis study of the UV spectrum and kinetics of reactions of the acetylperoxy radical, *J. Chem. Soc. Faraday Trans.*, **89**(16), 2993-2997, 1993.
- Cantrell, C. A., J. A. Davidson, A. H. McDaniel, R. E. Shetter, and J. G. Calvert, Temperature-dependent formaldehyde cross-sections in the near-ultraviolet spectral region, *J. Phys. Chem.*, **94**, 3902-3908, 1990.
- Carter, W. P. L., A detailed mechanism for the gas-phase atmospheric reactions of organic compounds, *Atmos. Environ.*, **24A**, 481-518, 1990.
- Carter, W. P. L., Computer modeling of environmental chamber studies of maximum incremental reactivities of volatile organic compounds, *Atmos. Environ.*, **29**, 2513-2527, 1995.
- Carter, W. P. L., Condensed atmospheric photooxidation mechanisms for isoprene, *Atmos. Environ.*, **30**, 4275-4290, 1996.
- Carter, W. P. L., and R. Atkinson, Alkyl nitrate formation from the atmospheric photooxidation of alkanes: A revised estimation method, *J. Atmos. Chem.*, **8**, 165-173, 1989.
- Carter, W. P. L., and R. Atkinson, Development and evaluation of a detailed mechanism for the atmospheric reactions of isoprene and NO_x, *Int. J. Chem. Kinet.*, **28**, 497-530, 1996.
- Carter, W. P. L., D. Luo, I. L. Malkina, and D. Fitz, *The University of California, Riverside Environmental Chamber Data Base for Evaluating Oxidant Mechanisms*, vol. 1, Univ. of Calif. Press, Riverside, 1995a.
- Carter, W. P. L., D. Luo, I. L. Malkina, and D. Fitz, *The University of California, Riverside Environmental Chamber Data Base for Evaluating Oxidant Mechanisms*, vol. 2, Univ. of Calif. Press, Riverside, 1995b.
- Chin, M., D. J. Jacob, G. M. Gardener, M. S. Foreman-Fowler, P. A. Spiro, and D. L. Savoie, A global three-dimensional model of tropospheric sulfate, *J. Geophys. Res.*, **101**, 18,667-18,690, 1996.
- DeMore, W. B., S. P. Sander, D. M. Golden, R. F. Hampson, M. J. Kurylo, C. J. Howard, A. R. Ravishankara, C. E. Kolb, and M. J. Molina, *Chemical kinetics and photochemical data for use in stratospheric modeling*, Eval. **12**, NASA, Jet Propul. Lab. Calif. Inst. of Technol., Pasadena, 1997.
- Dodge, M. C., Combined use of modeling techniques and smog chamber data to derive ozone-precursor relationships, Rep. EPA-600/3-77/001a, U.S. Environmental Protection Agency, Research Triangle Park, N. C., 1977.
- Erickson, D. J., III, J. J. Walton, S. J. Ghan, and J. E. Penner, Three-dimensional modeling of the global atmospheric sulfur cycle: A first step, *Atmos. Environ.*, **25A**, 2513-2520, 1991.
- Feichter, J., E. Kjellstrom, H. Rodhe, F. Dentener, J. Lelieveld, and G.-J. Roelofs, Simulation of the tropospheric sulfur cycle in a global climate model, *Atmos. Environ.*, **30**, 1693-1707, 1996.
- Gery, M. W., G. Z. Whitten and J. P. Killus, Development and testing of the CBM-IV for urban and regional modeling, Rep. EPA-600/3-88/012, U.S. Environ. Prot. Agency, Research Triangle Park, N. C., 1988.
- Gery, M. W., G. Z. Whitten, J. P. Killus, and M. C. Dodge, A photochemical kinetics mechanism for urban and regional scale computer modeling, *J. Geophys. Res.*, **94**, 12,925-12,956, 1989.
- Grosjean, E., and D. Grosjean, Carbonyl products of the gas phase reaction of ozone with symmetrical alkenes, *Environ. Sci. Technol.*, **30**, 2036-2044, 1996a.
- Grosjean, E., and D. Grosjean, Carbonyl products of the gas-phase reaction of ozone with 1-alkenes, *Atmos. Environ.*, **30**, 4107-4113, 1996b.
- Grosjean, E., and D. Grosjean, Gas phase reaction of alkenes with ozone: Formation yields of primary carbonyls and biradicals, *Environ. Sci. Technol.*, **31**, 2421-2427, 1997.
- Grosjean, D., E. Grosjean, and E. L. Williams II, Atmospheric chemistry of olefins: A product study of the ozone-alkene reaction with cyclohexane added to scavenge OH, *Environ. Sci. Technol.*, **28**, 186-196, 1994.
- Grosjean, E., D. Grosjean, and J. H. Seinfeld, Atmospheric chemistry of 1-octene, 1-decene, and cyclohexene: Gas-phase carbonyl and peroxyacyl nitrate products, *Environ. Sci. Technol.*, **30**, 1038-1047, 1996.
- Hatakeyama, S., H. Bandow, M. Okuda, and H. Akimoto, Reactions of CH₂OO and CH₂(¹A₁) with H₂O in the gas phase, *J. Phys. Chem.*, **85**, 2249-2254, 1981.
- Hatakeyama, S., H. Kobayashi, and H. Akimoto, Gas-phase oxidation of SO₂ in the ozone-olefin reactions, *J. Phys. Chem.*, **88**, 4736-4739, 1984.
- Hatakeyama, S., H. Kobayashi, Z.-Y. Lin, H. Takagi, and H. Akimoto, Mechanism for the reaction of CH₂OO with SO₂, *J. Phys. Chem.*, **90**, 4131-4135, 1986.
- Hess, G. D., F. Carnovale, M. E. Cope, and G. M. Johnson, The evaluation of some photochemical smog reaction mechanisms, I, Temperature and initial concentration effects, *Atmos. Environ.*, **26A**, 625-641, 1992a.
- Hess, G. D., F. Carnovale, M. E. Cope, and G. M. Johnson, The evaluation of some photochemical smog reaction mechanisms, II, Initial addition of alkanes and alkenes, *Atmos. Environ.*, **26A**, 643-651, 1992b.
- Hess, G. D., F. Carnovale, M. E. Cope, and G. M. Johnson, The evaluation of some photochemical smog reaction mechanisms, III, Dilution and emissions effects, *Atmos. Environ.*, **26A**, 653-659, 1992c.
- Horic, O., and G. K. Moortgat, Decomposition pathways of the excited Criegee intermediates in the ozonolysis of simple alkenes, *Atmos. Environ.*, **25A**, 1881-1896, 1991.
- Horie, O., P. Neeb, S. Limbach, and G. K. Moortgat, Formation of formic acid and organic peroxides in the ozonolysis

- of ethene with added water vapor, *Geophys. Res. Lett.*, **21**, 1523-1526, 1994.
- Jeffries, H. E., R. M. Kamens, K. G. Sexton, and A. A. Gerhardt, Outdoor smog chamber experiments to test photochemical models, *Rep. EPA-600/3-82/016*, U.S. Environ. Prot. Agency, Research Triangle Park, N. C., 1982.
- Jeffries, H. E., K. G. Sexton, T. P. Morris, M. Jackson, R. G. Goodman, R. M. Kamens, and M. Holleman, Outdoor smog chamber experiments using automobile exhaust, *Rep. EPA-600/3-85/032*, U.S. Environ. Prot. Agency, Research Triangle Park, N. C., 1985.
- Jeffries, H. E., M. W. Gery, and W. P. L. Carter, Protocols for evaluating oxidant mechanisms used in urban and regional models, *Coop. Agreement 815779*, U.S. Environ. Prot. Agency, Research Triangle Park, N. C., 1987.
- Jenkin, M. E., S. M. Saunders, and M. J. Pilling, The tropospheric degradation of volatile organic compounds: A protocol for mechanism development, *Atmos. Environ.*, **31**, 81-104, 1997.
- Kirchner, F., and W. R. Stockwell, Effect of peroxy radical reactions on the predicted concentrations of ozone, nitrogenous compounds, and radicals, *J. Geophys. Res.*, **101**, 21,007-21,022, 1996.
- Langner, J., and H. Rodhe, A global three-dimensional model of the tropospheric sulfur cycle, *J. Atmos. Chem.*, **13**, 225-263, 1991.
- Lurmann, F. W., W. P. L. Carter, and L. A. Coyner, A surrogate species chemical reaction mechanism for urban-scale air quality simulation models, *Rep. EPA/600/3-87/014*, U.S. Environ. Prot. Agency, Research Triangle Park, N. C., 1987.
- Madronich, S., and J. G. Calvert, Permutation reactions of organic peroxy radicals in the troposphere, *J. Geophys. Res.*, **95**, 5697-5715, 1990.
- Martinez, R. D., A. A. Buitrago, N. W. Howell, C. H. Hearn, and J. A. Joens, The near U.V. absorption spectra of several aliphatic aldehydes and ketones at 300 K, *Atmos. Environ.*, **26A**, 785-792, 1992.
- McRae, G. J., W. R. Goodin, and J. H. Seinfeld, Development of a second-generation mathematical model for urban air pollution, I, *Atmos. Environ.*, **16**, 16,679-16,696, 1982.
- Middleton, P., W. R. Stockwell, and W. P. L. Carter, Aggregation and analysis of volatile organic compound emissions for regional modeling, *Atmos. Environ.*, **24A**, 1107-1133, 1990.
- Moortgat, G. K., W. Klippel, K. H. Mobus, W. Seiler, and P. Warneck, Laboratory measurement of photolytic parameters for formaldehyde, *Final Rep. FAA-EE-80-47*, Off. of Environ. and Energy, Fed. Aviat. Admin., Washington, D. C., 1980.
- Neeb, P., O. Horie, and G. K. Moortgat, The nature of the transitory product in the gas-phase ozonolysis of ethene, *Chem. Phys. Lett.*, **246**, 150-156, 1995.
- Neeb, P., O. Horie, and G. K. Moortgat, Gas-phase ozonolysis of ethene in the presence of hydroxylic compounds, *Int. J. Chem. Kinet.*, **28**, 721-730, 1996.
- Neeb, P., F. Sauer, O. Horie, and G. K. Moortgat, Formation of hydroxymethyl hydroperoxide and formic acid in alkene ozonolysis in the presence of water vapour, *Atmos. Environ.*, **31**, 1417-1423, 1997.
- Niki, H., P. D. Maker, C. M. Savage, and L. P. Breitenbach, Fourier transform IR spectroscopic observation of propylene ozonide in the gas phase reaction of ozone—cis-2-butene—formaldehyde, *Chem. Phys. Lett.*, **46**, 327-330, 1977.
- Niki, H., P. D. Maker, C. M. Savage, and L. P. Breitenbach, A FT-IR study of a transitory product in the gas-phase ozone-ethylene reaction, *J. Phys. Chem.*, **85**, 1024-1027, 1981.
- Paulson, S. E., and J. H. Seinfeld, Development and evaluation of a photooxidation mechanism for isoprene, *J. Geophys. Res.*, **97**, 20,703-20,715, 1992.
- Pham, M., J.-F. Müller, G. P. Brasseur, C. Granier, and G. Mégie, A three-dimensional study of the tropospheric sulfur cycle, *J. Geophys. Res.*, **100**, 26,061-26,092, 1995.
- Placet, M., R. E. Battye, F. C. Fehsenfeld, and G. W. Bassett, Emissions involved in acidic deposition, in *Acidic Deposition: State of the Science and Technology, Rep. 1*, U.S. Nat. Acid Precip. Assess. Program, Washington, D. C., 1991.
- Simonaitis, R., J. F. Mcagher, and E. M. Bailey, Evaluation of the condensed Carbon Bond (CB-IV) mechanism against smog chamber data at low VOC and NO_x concentrations, *Atmos. Environ.*, **31**, 27-43, 1997.
- Stockwell, W. R., A homogeneous gas-phase mechanism for use in a regional acid depositional model, *Atmos. Environ.*, **20**, 1615-1632, 1986.
- Stockwell, W. R., On the HO₂ + HO₂ reaction: Its misapplication in atmospheric chemistry models, *J. Geophys. Res.*, **100**, 11,695-11,698, 1995.
- Stockwell, W. R., P. Middleton, J. S. Chang, and X. Tang, The second-generation regional acid deposition model chemical mechanism for regional air quality modeling, *J. Geophys. Res.*, **95**, 16,343-16,367, 1990.
- Stockwell, W. R., F. Kirchner, and M. Kuhn, A new mechanism for regional atmospheric chemistry modeling, *J. Geophys. Res.*, **102**, 25,847-25,879, 1997.
- Su, F., J. G. Calvert, and J. H. Shaw, A FT-IR spectroscopic study of the ozone-ethene reaction mechanism in O₂-rich mixtures, *J. Phys. Chem.*, **84**, 239-246, 1980.
- Tuazon, E. C., S. M. Aschmann, J. Arey, and R. Atkinson, Products of the gas-phase reactions of O₃ with a series of methyl-substituted ethenes, *Environ. Sci. Technol.*, **31**, 3004-3009, 1997.
- Wayne, R. P., *et al.*, The nitrate radical: Physics, chemistry, and the atmosphere, *Atmos. Environ.*, **25A**, 1-203, 1991.
- Whitten, G. Z., H. Hogo, and J. P. Killus, The carbon-bond mechanism: A condensed kinetic mechanism for photochemical smog, *Environ. Sci. Technol.*, **18**, 280-287, 1980.
- Zimmerman, J. and D. Poppe, A supplement for the RADM2 chemical mechanism: The photooxidation of isoprene, *Atmos. Environ.*, **30**, 1255-1269, 1996.

L. K. Peters, Department of Chemical Engineering, Virginia Polytechnic Institute and State University, Blacksburg, VA 24061. (petersl@vt.edu)

R. A. Zaveri, Pacific Northwest National Laboratory, MSIN K9-30, P.O. Box 999, Richland, WA 99352. (Rahul.Zaveri@pnl.gov)

(Received February 4, 1999; revised August 9, 1999; accepted August 12, 1999.)